Journal of Inflammation Research

Dovepress
Taylor & Francis Group

Open Access Full Text Article

ORIGINAL RESEARCH

Deciphering the Therapeutic Mechanisms of Banxia Xiexin Decoction Against Ulcerative Colitis: Targeting Pyroptosis and Necroptosis

Jie Lu[1,*], Kun Liang[1,*], Li Zhang[1], Bo Cui[1], Lisha You[1], Rui An[1], Cheng Hu[2], Xinhong Wang[1]

[1]School of Pharmacy, Shanghai University of Traditional Chinese Medicine, Shanghai, 201203, People's Republic of China; [2]Innovation Center for Traditional Chinese Medicine, Shanghai University of Traditional Chinese Medicine, Shanghai, 201203, People's Republic of China

*These authors contributed equally to this work

Correspondence: Xinhong Wang; Rui An, School of Pharmacy, Shanghai University of Traditional Chinese Medicine, Shanghai, 201203, People's Republic of China, Email wangxinh6020@126.com; anruimw@126.com

Purpose: Previous studies have highlighted a strong association between programmed cell death and ulcerative colitis (UC). Banxia Xiexin decoction (BXD) is a thoroughly validated formula with an extensive history of clinical application for treating UC. However, it remains unclear whether BXD regulates pyroptosis and necroptosis in UC. This study focused on pyroptosis and necroptosis to investigate the underlying mechanisms of BXD on UC.

Material and Methods: The therapeutic effects of BXD were evaluated in a dextran sulfate sodium (DSS)-induced colitis mouse model. To identify key signaling pathways, transcriptomics and proteomics were performed, followed by the validation of these pathways using Western blotting, immunohistochemistry, and immunofluorescence in vivo and in vitro. The bioactive components of BXD were screened through pharmacodynamic experiments, molecular docking, and surface plasmon resonance (SPR) analysis.

Results: BXD significantly alleviated UC symptoms by reducing inflammatory levels and improving intestinal barrier function. Multi-omics analyses demonstrated a significant alteration in pyroptosis- and necroptosis-related signaling pathways following BXD intervention. BXD suppressed pyroptosis through the P2RX7/NEK7 pathway and necroptosis via the TNFR1/RIPK3 pathway in the colons of UC model mice and in LPS+TNF-α-induced NCM460 cells. The screening of active ingredients revealed that baicalin and glycyrrhizic acid significantly affected LDH release and IL-1β levels. Molecular docking and SPR analyses demonstrated that baicalin targeted P2RX7 with high affinity and that glycyrrhizic acid targeted TNFR1 with moderate affinity.

Conclusion: BXD ameliorates inflammation and intestinal barrier dysfunction in UC by suppressing pyroptosis through the P2RX7/NEK7 pathway and necroptosis via the TNFR1/RIPK3 pathway. Baicalin and glycyrrhizic acid are identified as the pharmacodynamic components responsible for these therapeutic effects. These findings can provide molecular mechanisms and a material basis for the clinical application of BXD in the treatment of UC.

Keywords: ulcerative colitis, Banxia Xiexin decoction, multi-omics analyses, pyroptosis, necroptosis

Introduction

Ulcerative colitis (UC) is a persistent gastroint5estinal condition marked by cycles of recurring inflammation and remission.[1] UC manifests clinically as ulcers, severe bleeding, diarrhea, and abdominal pain.[2] The etiology of UC is linked to intestinal barrier disruption, which triggers aberrant activation of innate immune pathways.[3] Recent investigations have highlighted the crucial role of programmed cell death (PCD) in the pathophysiology of UC.[4] PCD, a critical biological process for maintaining tissue homeostasis, regulates cell fate through several mechanisms, including apoptosis, pyroptosis, necroptosis, and ferroptosis. Proper regulation of PCD is essential for intestinal epithelial cell renewal and repair, as well as for maintaining immune cell balance.[5] Accumulating evidence indicates that during acute flares of UC, different forms of PCD are upregulated in the intestinal tissues of patients.[6] Specifically, pyroptosis and necroptosis, both proinflammatory types of PCD, exacerbate intestinal inflammation and disrupt intestinal homeostasis.

Received: 9 September 2025
Accepted: 2 December 2025
Published: 16 December 2025

Graphical Abstract

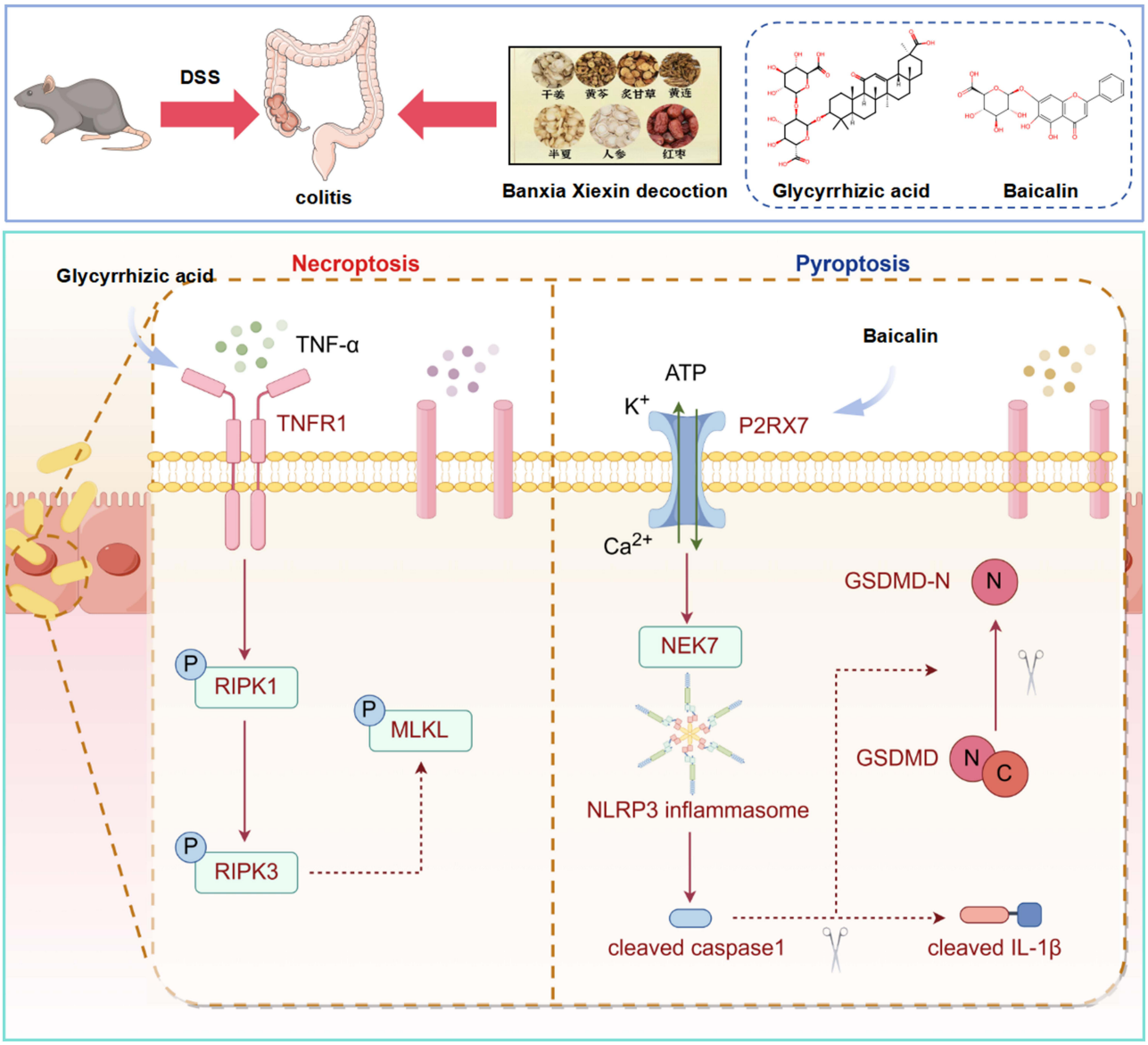

As an inflammatory variant of PCD, pyroptosis is typically activated by inflammasomes and executed by GSDMD.[7] Necroptosis, which involves necrotic morphological features, is regulated by MLKL.[8] Pyroptosis and necroptosis both induce the creation of membrane holes, facilitating the discharge of intracellular contents and leading to cell death. Excessive pyroptosis and necroptosis in the colon compromise barrier integrity and initiate inflammatory cascades, hence contributing to the pathophysiology of UC.[9] This dual amplification of inflammation and epithelial disruption positions pyroptosis and necroptosis as attractive therapeutic targets for UC intervention.

Within this context, traditional Chinese medicine (TCM) has drawn mounting attention on account of its multi-target and holistic regulatory effects in UC.[10] Banxia Xiexin decoction (BXD) is a prominent herbal formula originating from *Shanghan Lun*. BXD has a longstanding history of clinical application in addressing damp-heat syndrome.[11] UC is classified as a form of damp-heat syndrome in TCM theory.[12] In current clinical practice, BXD has shown significant effectiveness in the management of UC, alleviating clinical symptoms.[13,14] Previous studies have demonstrated that its

therapeutic effects on experimental colitis may be mediated through mechanisms such as regulating inflammatory cytokines,[15] enhancing immunomodulation,[16] and modulating the intestinal microbiota.[17] BXD consists of seven herbs: Pinelliae Rhizoma Preparatum (Banxia), Zingiberis Rhizoma (Ganjiang), Scutellariae Radix Georgi (Huangqin), Coptidis Rhizoma (Huanglian), Glycyrrhizae Radix Preparata (Gancao), Ginseng Radix (Renshen), and Jujubae Fructus (Dazao). The bioactive components in BXD have demonstrated efficacy against UC and resistance to PCD.[18,19] Ginsenoside Rg3, for instance, mitigates colitis by inhibiting the NLRP3 inflammasome, hence preventing pyroptosis.[20] Similarly, scutellarin suppresses mitochondrial damage and inhibits PANoptosis, which in turn mitigates inflammatory disorders.[9] It is plausible that the anti-colitic effects of BXD arise from the synergistic actions of its various components. Nonetheless, despite existing literature, the precise processes and roles of BXD to UC treatment remain ambiguous.

This study was designed to evaluate the therapeutic potency of BXD in UC, clarify its primary mechanisms, and identify its potential material basis, with particular attention to pyroptosis and necroptosis. This study provides a strong scientific foundation for the therapeutic application of BXD in the therapy of UC.

Materials and Methods

Preparation of BXD

BXD consists of *Pinellia ternate* (Thunb.) Breit. (NO.PR-230403), *Zingiber officinale* Rosc. (NO.ZR-230423), *Scutellaria baicalensis* Georgi (NO.SR-230111), *Coptis chinensis* Franch. (NO.CR-230408), *Glycyrrhiza uralensis* Fisch. (NO.GR-230315), *Panax ginseng* C. A. Mey. (NO.GR-230212) and *Ziziphus jujuba* Mill. (NO.JF-230419) at a weight ratio of 12:9:9:3:9:9:6. All medicinal materials were acquired from Shanghai Kangqiao Traditional Chinese Medicine Co., Ltd. All the medicinal materials were boiled twice, ten times the volume of distilled water, for 45 min per extraction. The combined filtrates were concentrated to 0.5 g/mL. The BXD was freeze-dried to obtain powdered products, and stored at 4°C. BXD was dissolved in phosphate-buffered saline (PBS) and thoroughly mixed prior to animal experiment. The analysis detail of BXD was presented in Supplementary Methods.

Animals

Male C57BL/6J mice (8–10 weeks of age, 20–24 g) were procured from Shanghai Jihui Laboratory Animal Care Co., Ltd. The mice were maintained in groups under specific pathogen-free settings (22±2°C, 50±10% humidity, 12 h light/dark cycle) at the Experimental Animal Centre of Shanghai University of Traditional Chinese Medicine. All methods received approval from the Ethics Review Committee of Shanghai University of Traditional Chinese Medicine (Approval No. PZSHUTCM2305150006). All animal experiments conducted in this study were performed in compliance with the ARRIVE guidelines.

Dextran Sulfate Sodium (DSS)-Induced Models and BXD Therapy

Sixty mice were randomly assigned to six groups: the control, DSS, 5-amino salicylic acid (5-ASA), BXD-L, BXD-M, and BXD-H groups, with ten mice per group (n=10). On the basis of the clinically used human dose and its conversion for mice, the medium dose of BXD was 5.8 g/kg/d, and the dose of 5-ASA (S30083, Yuanye Biotechnology, Shanghai) was 0.2 g/kg/d. Low and high doses of BXD were set at 2.9 g/kg/d and 11.6 g/kg/d, respectively, on the basis of the two-fold correlation. Following a 7-day acclimatization phase, all mice, with the exception of those in the control group, were administered a 2.5% DSS solution ad libitum for seven days. From day 0 to day 10, each group received intragastric administrations of the corresponding drugs at various concentrations or a volume-equivalent PBS. Daily monitoring was conducted for body weight, stool consistency, and fecal blood. Disease activity index (DAI) and hematoxylin and eosin (H&E) histopathology scores were evaluated based on previous studies.[21] On day 10, the mice were euthanized with zoletil 50 and xylazine, and the samples were harvested for subsequent analyses.

Histological Analysis

The staining of H&E, alcian blue (AB), and periodic acid schiff (PAS) were performed on the 3 μm colon sections fixed in 4% paraformaldehyde and embedded in paraffin. The quantification of goblet cells and mucus levels in the colon was conducted utilizing ImageJ 1.54j (National Institutes of Health, USA).

Immunohistochemistry and Immunofluorescence Staining

The paraffin slices were made as depicted in section 2.5. For immunohistochemistry, the sections were subjected to an endogenous peroxidase blocking solution for 35 min, and overnight incubation at 4°C with in the presence of antibodies p-MLKL (1:100, ET1705-51, Huaan) and GSDMD-N (1:100, HA721144, Huaan) followed by subsequent hematoxylin immunostaining. For immunofluorescence, the sections were subjected to primary antibodies ZO-1 (1:500, YM8448, Immunoway), GSDMD-N (1:100, YT7991, Immunoway), and p-MLKL (1:100, ET1705-51, Huaan). The slices were subjected to an immunofluorescent secondary antibody for 1 h, and DAPI staining for 10 min. For TdT mediated dUTP nick end labeling (TUNEL) staining, the TUNEL labeling working solution (G1502, Servicebio) was applied to the slides.

Enzyme-Linked Immunosorbent Assay (ELISA)

Serum concentrations of interleukin (IL)-6, IL-17, chemokine (C-X-C motif) ligand (CXCL)1, tumor necrosis factor (TNF)-α, and lipopolysaccharides (LPS); colon concentrations of IL-1β, IL-18, and myeloperoxidase (MPO); and cell supernatant levels of IL-1β and high-mobility group box 1 (HMGB1) were determined utilizing commercial ELISA kits (ABclonal, Shanghai).

Transcriptomics Analysis

Total RNA was isolated with TRIzol Reagent and analyzed by the NanoDrop2000 (Thermo Fisher, USA). Libraries were prepared, PCR-amplified, purified, and quantified. Sequencing was performed on the NovaSeq 6000 (Illumina, USA). Raw readings were processed with Cutadapt (v1.15) to obtain clean reads, and transcript expression was calculated using FPKM. Differentially expressed genes (DEGs) were identified with fold-change thresholds of $FC > 2$ or $FC < 0.5$ and $P\ adj < 0.05$ as the significance criterion.

Label-Free Quantitative Proteomics Analysis

Proteins from colon tissue were extracted using urea with a protease inhibitor cocktail, reduced with dithiothreitol for 1 h at 57°C, and alkylated with iodoacetamide for 40 min. Proteins were digested overnight with trypsin (V511B, Promega) and purified through the FASP method. Proteomic profiling was performed on a nanoflow HPLC Easy-nLC 1000 coupled with an Orbitrap Fusion Lumos Mass Spectrometer. Data analysis was conducted using Fragpipe (v22.0, Nesvilab), and differentially expressed proteins (DEPs) with $FC > 1.2$ or $FC < 0.83$ and $P < 0.05$ were identified.

Bioinformatics Analyses

The Genescloud platform (https://www.genescloud.cn/home) was employed to perform principal component analysis (PCA) and Kyoto encyclopedia of genes and genomes (KEGG) enrichment analyses. The STRING database was utilized for protein-protein interaction (PPI) analysis with a confidence threshold set at > 0.7. Cytoscape 3.10.2 was employed to the visualization of the PPI network. Functional enrichment analysis was performed through Metascape (https://metascape.org/).

Cell Lines and Culture

The NCM460 cell line was purchased from BDBIO Co., Ltd. (Zhejiang, China). The cells were cultured in RPMI-1640 medium supplemented with 10% fetal bovine serum (FBS) and 1% penicillin-streptomycin (P/S) under standard conditions. In accordance with the literature, a modeling approach was employed to simulate PCD induced by UC.[22,23] NCM460 cells were primed with 1 μg/mL LPS (HY-D1056, MCE), 100 ng/mL TNF-α (C008, Novoprotein), and 20 μM nigericin (HY-127019, MCE) for 24 h. The concentrations of BXD (3.125, 6.25, and 12.5 μg/mL) were

rationally determined based on the CCK-8 assay and LDH assays. To monitor morphological changes across different groups, NCM460 cells were examined under a microscope, and corresponding images were acquired.

Cell Counting Kit-8 (CCK-8) and Lactate Dehydrogenase (LDH) Assays

Following treatment, the CCK-8 assay was utilized to assess cell proliferation (CT0001, SparkJade). Following a 30-minute incubation of the CCK-8 solution, the absorbance was assessed at 450 nm, and cell viability (%) was calculated accordingly. Cellular membrane integrity was evaluated by measuring LDH release using an LDH assay kit (MA0649, MeilunBio) at 490 nm, and LDH release (%) was calculated.

Annexin-V FITC/PI Flow Cytometry

After treatment, NCM460 cells were harvested and resuspended in 1× binding buffer. With the addition of FITC-Annexin V and PI dyes, the samples were incubated for 15 min and diluted with 1× binding buffer. The flow cytometry was conducted within 1 h.

Molecular Docking Simulation

Molecular docking was performed utilizing Autodock Vina version 1.1.2 software. The component structures were obtained from PubChem database (https://pubchem.ncbi.nlm.nih.gov/). Target proteins P2RX7 (PDB ID: 8tr7) and TNFR1 (PDB ID: 1ext) were retrieved from PDB database (https://www.pdb.org/). The active pockets of the inhibitors A839977 and balinatunfib were designated as binding sites to assess the binding potency of active components. The docking results were visualized via PLIP tool.

Surface Plasmon Resonance

For immobilization on CM7 chips, P2RX7 protein was dissolved and processed under the following parameters: 50 μg/mL, pH 4.0, flow rate 10 μL/min, and 25°C. Baicalin, berberine, coptisine, epiberberine, scutellarin, baicalein, chrysin, and glycyrrhizic acid were serially diluted with 1% DMSO buffer and injected at 30 μL/min for the contact phase and the dissociation phase. Binding data was acquired via the Biacore T200 evaluation software. For TNFR1, after the protein was solubilized and immobilized via the same protocol, the subsequent procedures were conducted as described above.

Western Blotting Analysis

Primary antibodies used included NF-κB p65 (1:2000, GB12142, Servicebio), p-NF-κB p65 (1:1000, 3033S, Cell Signaling technology), ZO-1 (1:2000, GB111402, Servicebio), P2RX7 (1:5000, 28,207-1-AP, Proteintech), NEK7 (1:10000, ab133514, Abcam), NLRP3 (1:1000, T55651S, Abmart), ASC (1:5000, 10,500-1-AP, Proteintech), caspase-1 (1:1000, ab179515, Abcam), GSDMD (1:5000, ab219800, Abcam), cleaved IL-1β (1:1000, 63124S, Cell Signaling technology), TNFR1 (1:500, 21,574-1-AP, Proteintech), p-RIPK1 (1:500, AP1314, ABclonal), RIPK1 (1:1000, A27859, ABclonal), p-RIPK3 (1:1000, 91702, Cell Signaling technology), RIPK3 (1:2000, YM8350, Immunoway), p-MLKL (1:1000, YP1884, Immunoway), MLKL (1:2000, YM8455, Immunoway), GADPH (1:50,000, 60,004-1-Ig, Proteintech), and β-actin (1:10000, GB11001, Servicebio), which were incubated overnight at 4°C. The membranes were incubated with an HRP-conjugated secondary antibody for 1 hour. All membranes were subjected to ECL detection reagents and subsequently analyzed with ImageJ.

Real-Time Quantitative PCR Assay

Total RNA was extracted from colon tissues using the TRIzol® Reagent (15596026, Thermo Fisher Scientific). Briefly, samples were homogenized in TRIzol reagent, mixed with chloroform, and centrifuged at 12,000 rpm for 15 min. The upper aqueous phase was collected, and RNA was precipitated with isopropanol, washed with 75% ethanol, and resuspended in RNase-free water. The purity and concentration of total RNA were determined using a NanoDrop 2000 spectrophotometer. Subsequently, complementary DNA (cDNA) was synthesized from 1 μg of total RNA using the SweScript All-in-One RT SuperMix for qPCR (G3337, Servicebio). Following cDNA synthesis, real-time qPCR was performed using the Universal Blue SYBR Green qPCR Master Mix (G3326, Servicebio). The following thermal cycling

conditions were used: initial denaturation at 95°C for 30 sec, followed by 40 cycles of denaturation at 95°C for 15 sec and annealing/extension at 60°C for 30 sec. The melting curve analysis was performed by heating from 65°C to 95°C at a rate of 0.5°C per sec with continuous fluorescence monitoring. The qPCR primer sequences were listed in Table 1, and the internal reference was GAPDH. The results were analyzed using the $2^{-\Delta\Delta Ct}$ method.

Statistical Analysis

The data were presented as mean±standard error of mean (SEM). For multiple group comparisons with normally distributed data and homogeneity of variance, one-way ANOVA followed by post-hoc Tukey's multiple comparisons test was employed. All the statistical analyses were performed with GraphPad Prism 8.4.3 software (GraphPad Software Inc., California, USA), with $P < 0.05$ considered statistically significant.

Results

Identification and Characterization of Chemical Components in BXD

UPLC-LTQ-Orbitrap-MS was employed to analyze the chemical composition of BXD. According to a previous study[24] and the 2020 Edition of the Chinese Pharmacopoeia specifications for the seven herbs in BXD, 23 components were identified in both positive and negative ion modes. Figure 1A illustrates the chemical structures of the 23 components, while Figure 1B presents the total ion chromatogram of BXD. Table 2 summarizes the UPLC-LTQ-Orbitrap-MS analysis results of the index components. Specifically, the following indices were detected: baicalin, a primary component of Scutellariae Radix; berberine, a key constituent of Coptidis Rhizoma; ginsenoside Rb1, ginsenoside Rg1, and ginsenoside Re, three representative components of Ginseng Radix; and glycyrrhizic acid, a major component of Glycyrrhizae Radix Preparata. This confirmed the stability of quality control for BXD.

BXD Alleviated Colitis Symptoms in DSS Mice

The therapeutic efficacy of BXD was assessed in a model of acute colitis induced by 2.5% DSS. Assessments of body weight and DAI scores demonstrated that the DSS-treated mice presented significant weight loss and an increased DAI after seven days relative to those of the control group. In contrast, BXD-M and BXD-H administration significantly mitigated weight loss, and exhibited a notable decrease in the DAI score (Figure 2A and B). Additionally, the colonic length was significantly greater in the BXD-M and BXD-H groups than in the DSS group (Figure 2C and D). HE staining revealed that DSS induced mucosal erosion (black arrow in Figure 2E), crypt destruction (red arrow in Figure 2E), and infiltration of inflammatory cells (blue arrow in Figure 2E). However, BXD-M and BXD-H effectively ameliorated colonic histopathological damage (Figure 2E). The histological scores also supported these findings (Figure 2F). These results suggested that BXD significantly ameliorated UC symptoms in mice.

Table 1 Sequences of the Primers Used for RT-qPCR

Gene	Primer	Gene Sequence (5'-3')
ZO-1	Sense primer	GGGAAAACCCGAAACTGATG
	antisense primer	GCTGTACTGTGAGGGCAACG
TNF-α	Sense primer	ACTCCAGGCGGTGCCTATGT
	antisense prime	GTGAGGGTCTGGGCCATAGAA
IL-6	Sense primer	CCACTCCCAACAGACCTGTCTA
	antisense prime	CTGCAAGCCAGTTTGGTAGCATC
GAPDH	Sense primer	CCTCGTCCCGTAGACAAAATG
	antisense primer	TGAGGTCAATGAAGGGGTCGT

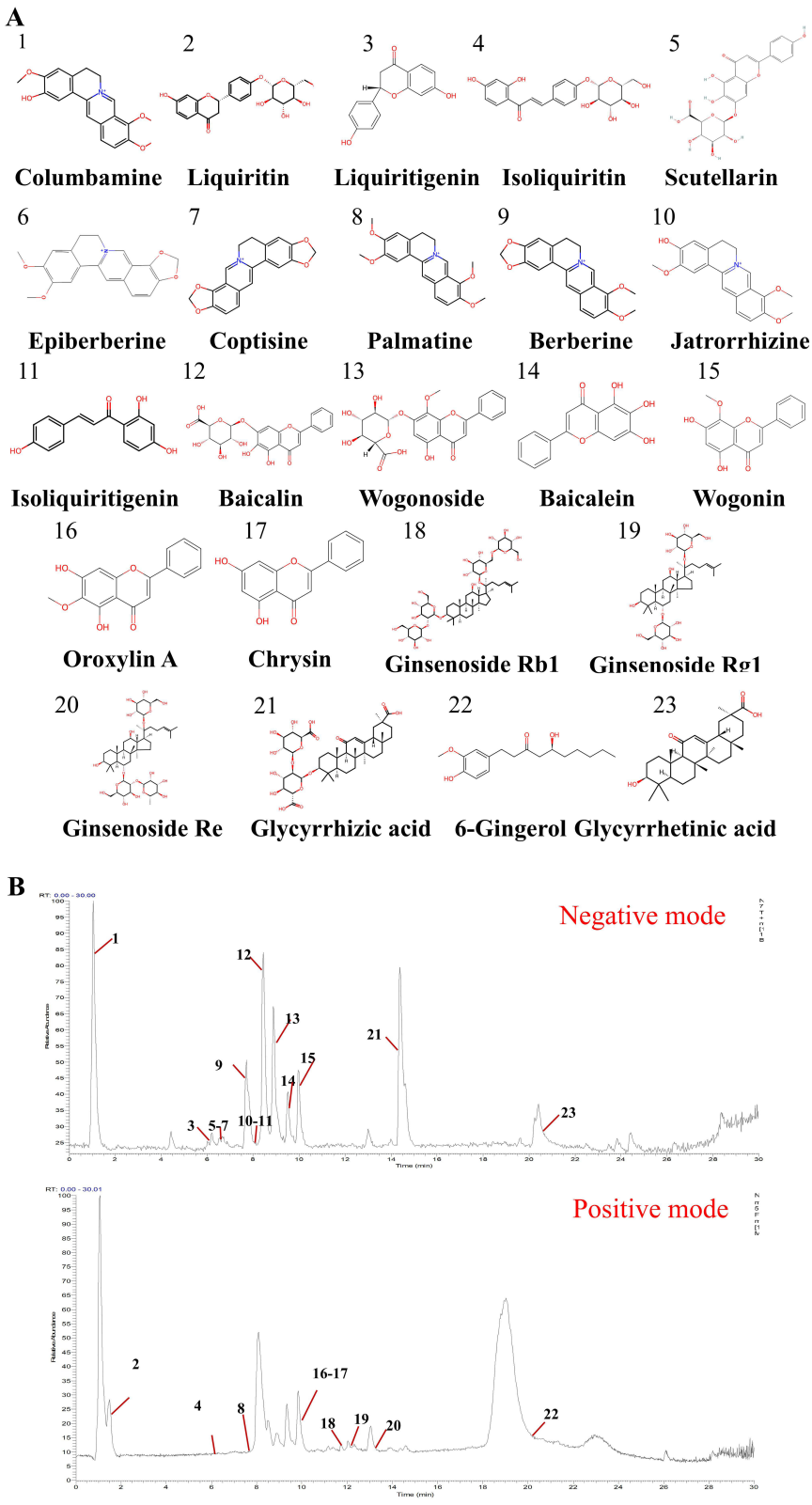

Figure 1 Chemical constituents of BXD. (**A**) Chemical structures of the main components in BXD. (**B**) Typical total ion chromatograms in positive and negative ion modes by UPLC-LTQ-Obitrap MS/MS.

https://doi.org/10.2147/JIR.S564333

Table 2 Chemical Components in BXD Identified by UPLC-LTQ-Orbitrap-MS

No	Compounds	RT (min)	Formula	Detected *m/z*	Error/ppm	Adduct	Herb Source
1	Columbamine	1.18	$C_{20}H_{20}NO_4$	321.03958	−1.0	$[M+H-H_2O]^+$	Coptidis Rhizoma
2	Liquiritin	1.39	$C_{21}H_{22}O_9$	417.11755	−3.7	$[M-H]^-$	Glycyrrhizae Radix
3	Liquiritigenin	6.03	$C_{15}H_{12}O_4$	257.08013	−2.8	$[M+H]^+$	Glycyrrhizae Radix
4	Isoliquiritin	6.17	$C_{21}H_{22}O_9$	417.11765	−3.5	$[M-H]^-$	Glycyrrhizae Radix
5	Scutellarin	6.24	$C_{21}H_{18}O_{12}$	463.08582	−3.0	$[M+H]^+$	Scutellariae Radix
6	Epiberberine	6.55	$C_{20}H_{18}NO_4$	336.12208	−2.9	$[M]^+$	Coptidis Rhizoma
7	Coptisine	6.86	$C_{19}H_{14}NO_4$	320.09084	−2.7	$[M]^+$	Coptidis Rhizoma
8	Palmatine	7.53	$C_{21}H_{22}NO_4$	351.13669	3.4	$[M-H]^-$	Coptidis Rhizoma
9	Berberine	7.72	$C_{20}H_{18}NO_4$	336.12208	−2.9	$[M+H]^+$	Coptidis Rhizoma
10	Jatrorrhizine	7.83	$C_{20}H_{20}NO_4$	338.13751	−3.5	$[M+H]^+$	Coptidis Rhizoma
11	Isoliquiritigenin	8.21	$C_{15}H_{12}O_4$	255.06569	−2.3	$[M+H]^+$	Glycyrrhizae Radix
12	Baicalin	8.44	$C_{21}H_{18}O_{11}$	447.09088	−3.0	$[M+H]^+$	Scutellariae Radix
13	Wogonoside	7.47	$C_{22}H_{20}O_{11}$	461.10654	−2.8	$[M+H]^+$	Scutellariae Radix
14	Baicalein	9.50	$C_{15}H_{10}O_5$	271.05945	−2.4	$[M+H]^+$	Scutellariae Radix
15	Wogonin	9.98	$C_{16}H_{12}O_5$	285.07509	−2.3	$[M+H]^+$	Scutellariae Radix
16	Oroxylin A	10.01	$C_{16}H_{12}O_5$	283.06023	−2.8	$[M-H]^-$	Scutellariae Radix
17	Chrysin	10.52	$C_{15}H_{10}O_4$	253.04986	−3.0	$[M-H]^-$	Scutellariae Radix
18	Ginsenoside Rb1	10.70	$C_{54}H_{92}O_{23}$	1107.61032	−0.1	$[M-H]^-$	Ginseng Radix
19	Ginsenoside Rg1	10.95	$C_{42}H_{72}O_{14}$	845.48623	7.3	$[M-H+CH_3OH]^-$	Ginseng Radix
20	Ginsenoside Re	13.37	$C_{48}H_{82}O_{18}$	946.55517	2.2	$[M-H]^-$	Ginseng Radix
21	Glycyrrhizic acid	13.87	$C_{42}H_{62}O_{16}$	823.40914	−2.9	$[M+H]^+$	Glycyrrhizae Radix
22	6-Gingerol	20.79	$C_{17}H_{26}O_4$	293.17838	8.6	$[M-H]^-$	Zingiberis Rhizoma
23	Glycyrrhetinic acid	20.85	$C_{30}H_{46}O_4$	453.33491	−3.0	$[M+H-H_2O]^+$	Glycyrrhizae Radix

BXD Inhibited Both Systemic and Colonic Inflammatory Responses in DSS Mice

In comparison to the control group, the DSS group exhibited significantly elevated serum levels of IL-6, IL-17, CXCL1 and TNF-α, along with increased colon levels of MPO, IL-1β and IL-18. As expected, BXD intervention markedly decreased the concentrations of these proinflammatory cytokines in the serum and colon (Figure 3A–G). qRT-PCR analysis demonstrated that BXD mitigated DSS-induced increases in the mRNA levels of TNF-α and IL-6 (Figure 3H and I). Furthermore, Western blotting revealed that DSS mice exhibited significantly increased NF-κB phosphorylation in the colon. BXD treatment reduced its phosphorylation level (Figure 3J), indicating that BXD significantly reduced the inflammatory response in DSS-related intestinal injury.

BXD Reversed DSS-Related Intestinal Barrier Impairment and Cell Death

Intestinal barrier dysfunction is a major pathogenic factor in UC. AB and PAS staining revealed that obvious decreases in the mucus layer thickness and goblet cell count in the in DSS group. In contrast to DSS, BXD-M and BXD-H significantly facilitated mucus secretion and reversed the reduction in goblet cell number (Figure 4A–C). To further assess intestinal integrity, the serum LPS levels was were measured via ELISA. The effectiveness of BXD-M and BXD-H was demonstrated by their ability to reduce elevated serum LPS levels in DSS-induced colitis (Figure 4D). Immunofluorescence analysis further confirmed a reduction in the expression of the colonic tight junction protein ZO-1 induced by DSS. However, BXD-H treatment reversed this reduction (Figure 4E). This observation accorded with RT-qPCR and Western blotting, which demonstrated elevated ZO-1 mRNA and protein levels in the colon. (Figure 4F–H). These findings demonstrated that BXD effectively maintains the intestinal chemical and mechanical barriers in response to external stimuli. Similarly, 5-ASA demonstrated a protective effect by attenuating intestinal barrier disruption. PCD has been implicated as a primary contributor to intestinal barrier dysfunction. To characterize cell death in the colon, TUNEL staining was performed. TUNEL staining demonstrated a marked increase in TUNEL positive cells in the DSS-treated group relative to the control group. BXD-M and BXD-H treatment significantly decreased the number of

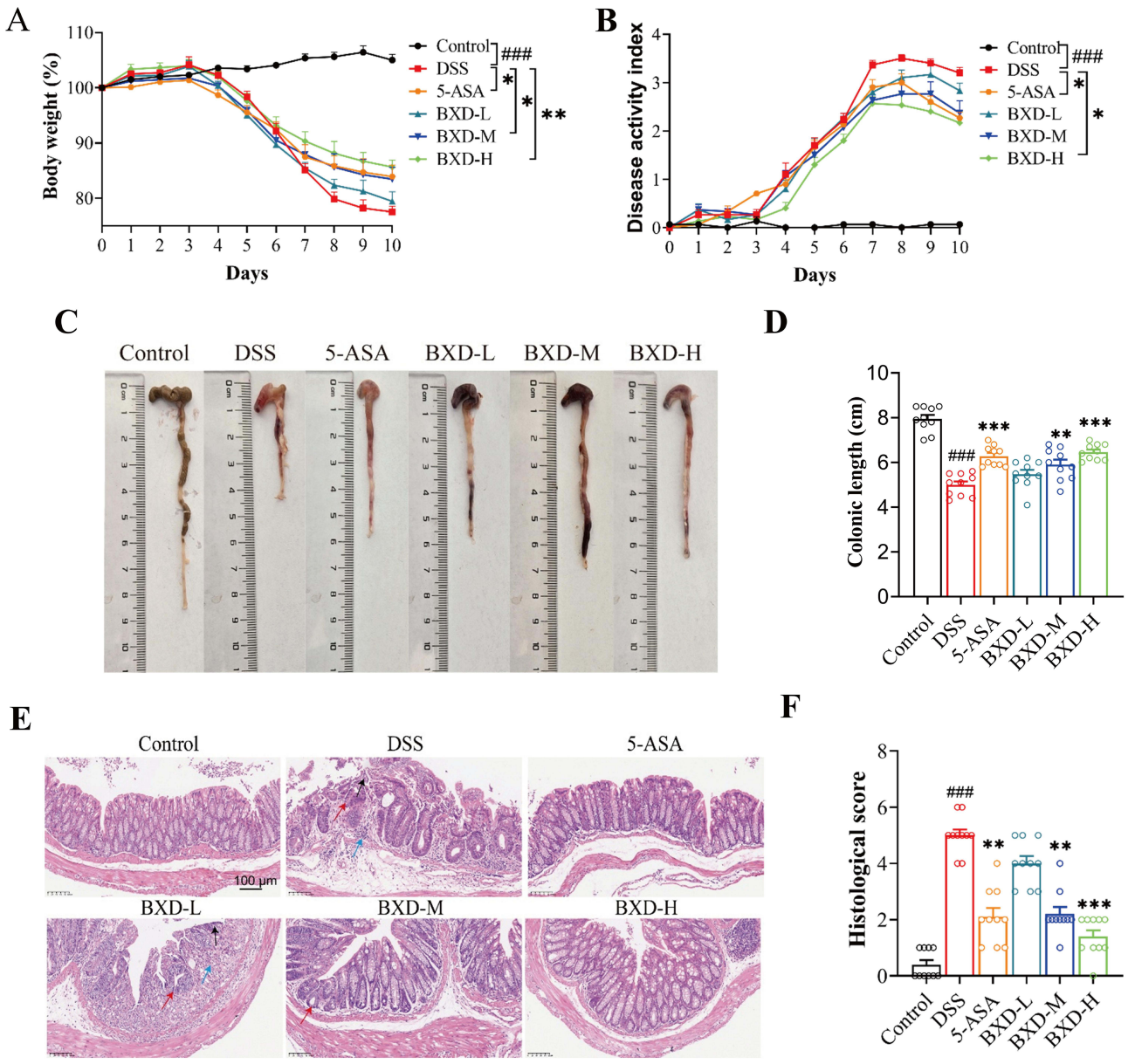

Figure 2 Therapeutic effects of BXD on acute experimental colitis. (**A**) Body weight curve. (**B**) DAI score. (**C**) Images depicting the colon following BXD treatment. (**D**) Colonic length (n=10). (**E**) Typical H&E staining of colon tissue sections. Scale bars represent 100 μm. (**F**) Histological scores (n=10). Data were presented as mean ±SEM. $^{\#\#\#}P < 0.001$ vs control group; $^{***}P < 0.001$, $^{**}P < 0.01$, $^{*}P < 0.05$ vs DSS group.

TUNEL-positive cells, demonstrating an inhibitory effect against DSS-induced colonic cell death (Figure 4I and J). The findings indicated that BXD may preserve intestinal function by potentially inhibiting cell death.

Transcriptomic and Proteomic Analysis

To comprehensively explore the underlying mechanism of BXD against UC, RNA sequencing and proteomics analysis were executed. Based on the findings from the animal pharmacodynamics experiments, we observed that BXD-H had a more consistent therapeutic effect. Therefore, this concentration was chosen for subsequent experiments. Colon tissues from the same mice were used for both the transcriptomic and proteomic analyses.

The transcriptomic profiles exhibited a clear differentiation among the control, DSS, and BXD groups in the PCA score scatter plots (Supplementary Figure 1). The volcano plots indicated that DSS treatment significantly modified gene

https://doi.org/10.2147/JIR.S564333

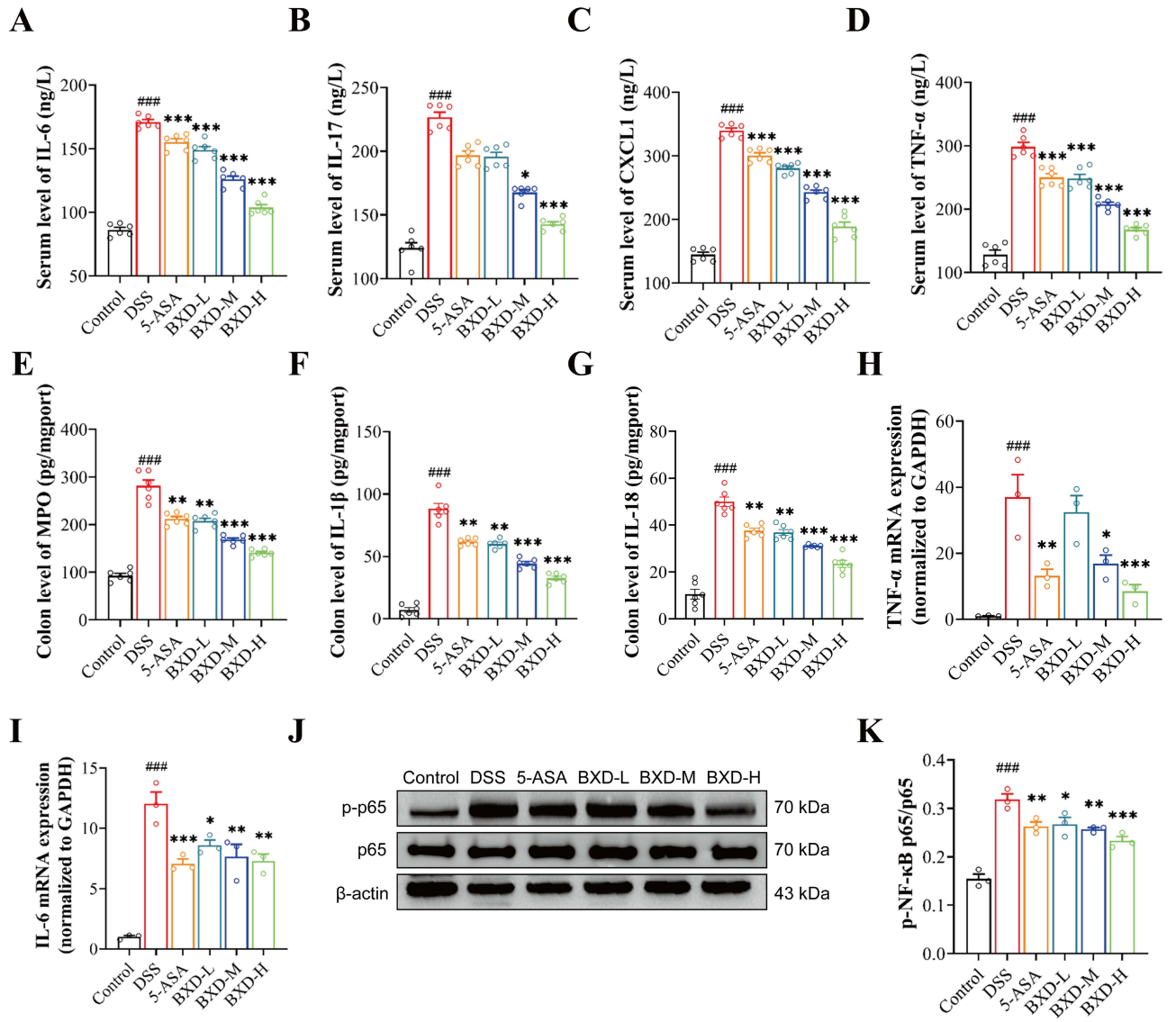

Figure 3 BXD inhibited systemic and colonic inflammatory cytokines in DSS-induced mice. (**A–D**) The levels of IL-6, IL-17, CXCL1, and TNF-α in the serum were measured by ELISA (n=6). (**E–G**) The levels of MPO, IL-1β, and IL-18 in the colon were measured by ELISA (n=6). (**H** and **I**) The mRNA expression of *IL-6* and *TNF-α* in the colon (n=3). (**J** and **K**) Western blot analysis of colonic NF-κB p65 and p-NF-κB p65. Data were presented as mean±SEM. $^{###}P < 0.001$ vs control group; $^{***}P < 0.001$, $^{**}P < 0.01$, $^{*}P < 0.05$ vs DSS group.

expression profiles, resulting in the downregulation of 1565 genes and the upregulation of 1054 genes. BXD treatment counteracted these alterations, leading to the downregulation of 690 genes and the upregulation of 2321 genes (Figure 5A, fold change > 2.0 or < 0.5, P adj< 0.05). Venn analysis revealed that 1471 key DEGs were co-regulated by BXD and DSS, with 454 downregulated DEGs and 1017 upregulated DEGs after BXD treatment (Supplementary Figure 2). KEGG pathway enrichment analysis demonstrated that these DEGs were predominantly involved in the NOD-like receptor signaling pathway, alpha-linolenic acid metabolism, linolenic acid metabolism, the IL-17 signaling pathway and the TNF signaling pathway (Figure 5B). These pathways are well recognized to participate in the immune response during UC.

Similar to the results of the transcriptomics analysis, PCA of proteomic analyses revealed distinct protein profiles among the control, DSS and BXD groups (Supplementary Figure 3). The volcano plots indicated that the DSS group exhibited 447 upregulated DEPs and 330 downregulated DEPs, and BXD treatment presented 418 upregulated DEPs and 557 downregulated DEPs (Figure 5C, fold change >1.2 or < 0.83, P < 0.05). Venn analysis revealed that 126 key DEPs

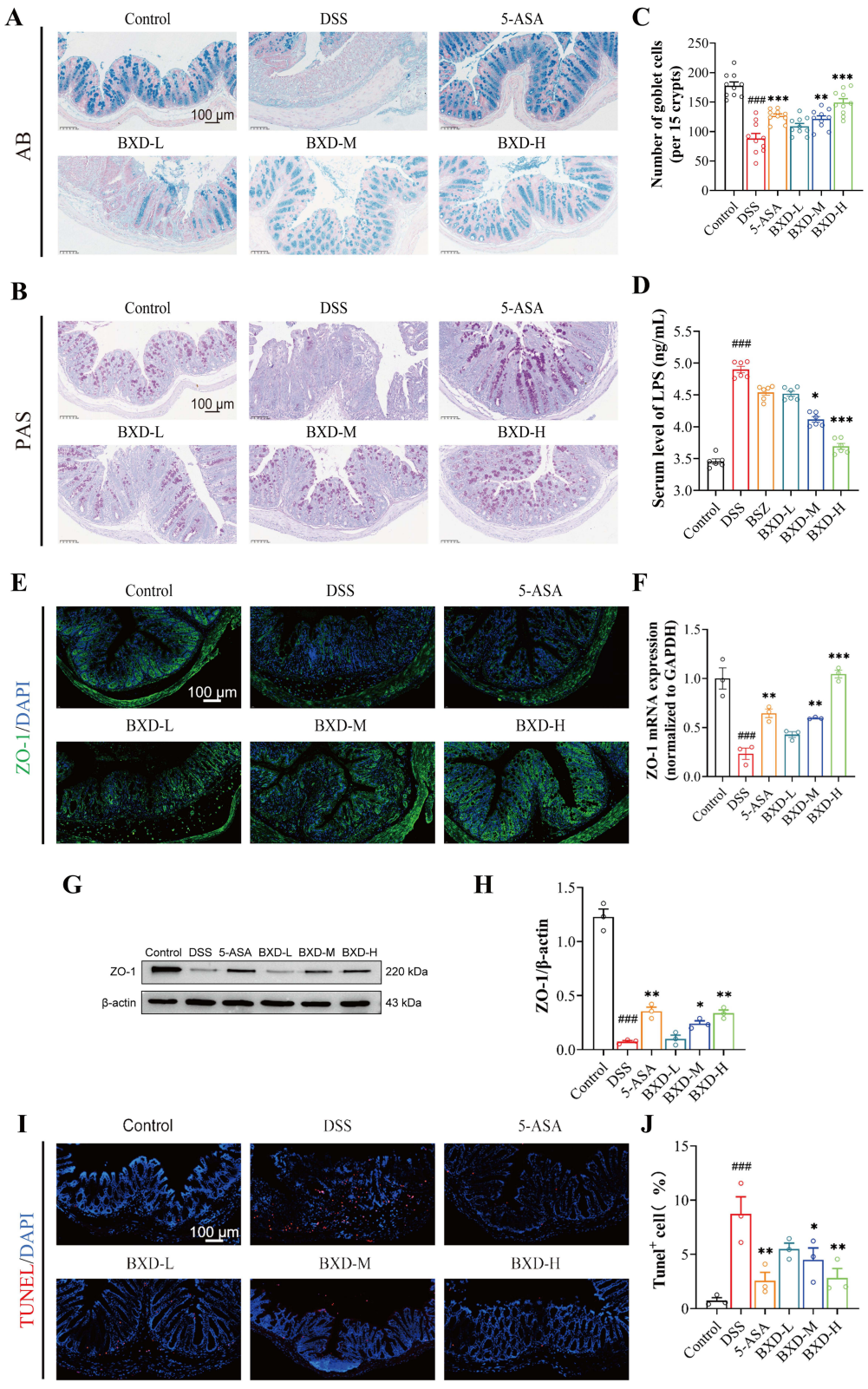

Figure 4 BXD improved intestinal barrier integrity in DSS-induced mice. (**A** and **B**) AB and PAS staining of the colon. Scale bars show 100 μm. (**C**) The quantity of goblet cells in the colon tissue (n=10). (**D**) The levels of LPS in the serum were measured by ELISA (n=6). (**E**) Immunofluorescence staining of ZO-1 in the colon. (**F**) The mRNA expression of *ZO-1* in the colon (n=3). (**G** and **H**) Western blot analysis of colonic ZO-1. (**I** and **J**) TUNEL staining and the relative density analysis. Scale bars show 100 μm. Data were presented as mean±SEM. $^{###}P < 0.001$ vs control group; $^{***}P < 0.001$, $^{**}P < 0.01$, $^{*}P < 0.05$ vs DSS group.

https://doi.org/10.2147/JIR.S564333

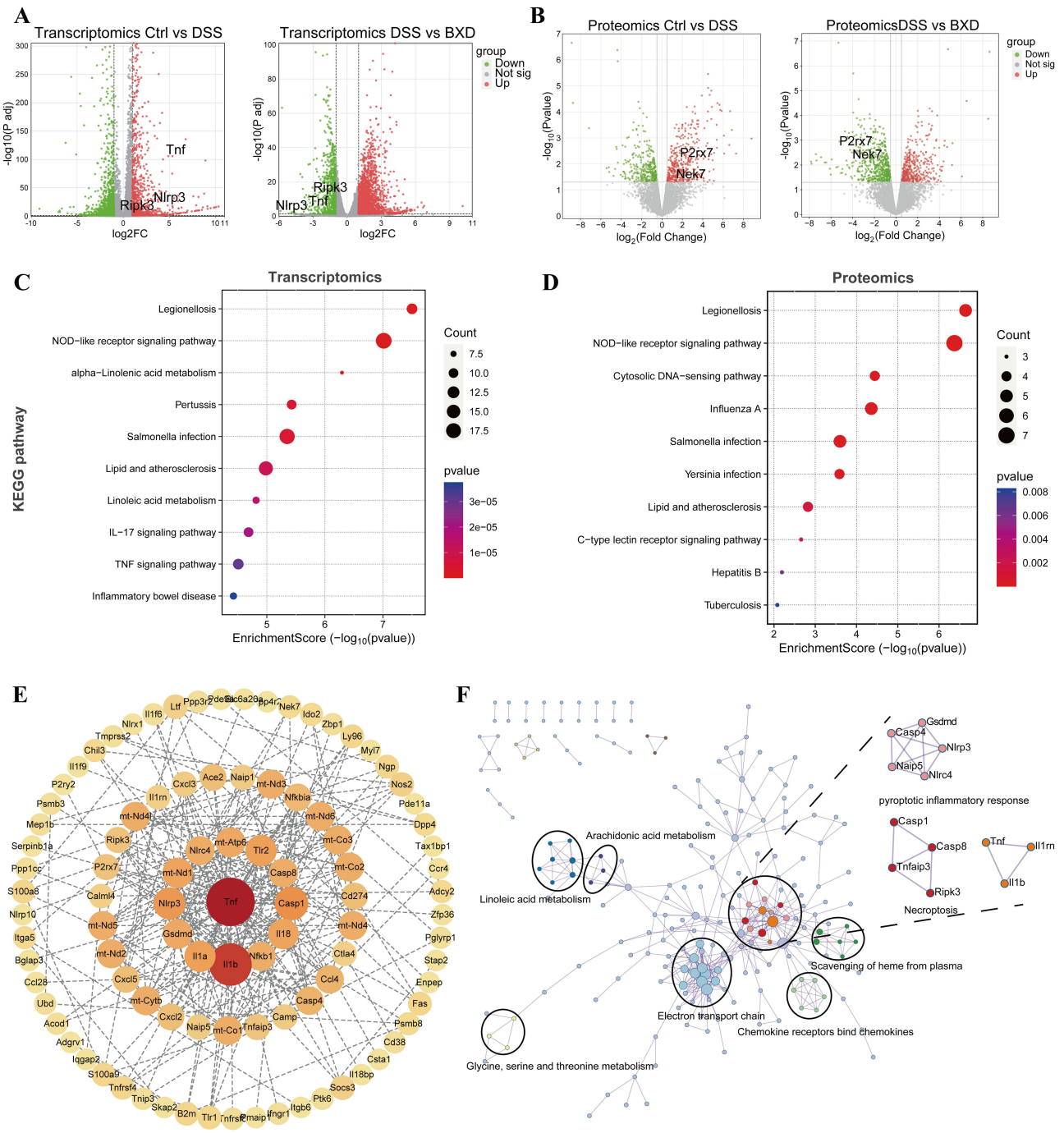

Figure 5 Transcriptomic and Proteomic analysis of DSS-induced mice following BXD treatment. (**A**) Volcano plots for DEGs. (**B**) Volcano plots for DEPs. (**C** and **D**) The KEGG pathways analysis of DEGs and DEPs. (**E**) Integrated analysis of protein-protein interaction networks for DEGs and DEPs. (**F**) Functional protein association network integrated with DEGs and DEPs.

were co-regulated by BXD and DSS, with 51 downregulated and 75 upregulated after BXD treatment (Supplementary Figure 4). Through KEGG pathway analysis, it was shown that these DEPs were mainly implicated in pathways related to immunity and inflammation, which included the NOD-like receptor signaling pathway, the cytosolic DNA-sensing pathway and the C-type lectin receptor signaling pathway (Figure 5D). Consistent with the transcriptomic findings, BXD primarily affected the protein expression of the NOD-like receptor signaling pathway, which is closely linked to inflammation and PCD and plays significant roles in the pathogenesis and progression of UC.

Table 3 Information of Key DEPs and DEGs Identified by Proteomics and Transcriptomics

UniPort ID	Gene Name	FC (DSS/Control)	FC (BXD/DSS)	P value	Category
Q3U593	*TNF*	22.12	0.46	7.32E-18	Transcriptomics
Q9QZL0	*RIPK3*	4.33	0.35	2.06E-13	transcriptomics
Q9Z1M0	*P2RX7*	6.02	0.10	0.00350	proteomics
Q9ES74	*NEK7*	4.32	0.13	0.00147	proteomics
Q8R4B8	*NLRP3*	7.43	0.42	9.04E-17	transcriptomics

To further comprehensively elucidate the transcriptomic and proteomic changes induced by BXD, we integrated the DEGs and DEPs to construct a protein-protein interaction (PPI) network. Topological analysis identified TNF (degree = 37) and IL-1β (degree = 29) as the key hub nodes in the PPI network, both of which are closely associated with inflammatory responses and PCD (Figure 5E). Functional enrichment analysis demonstrated that the DEGs and DEPs were primarily enriched in pyroptosis and necroptosis, both of which served as central nodes in the regulatory network (Figure 5F). These results suggested that the underlying mechanism of BXD may be closely associated with its resistance to PCD.

This transcriptomics and proteomics study revealed significant inhibition of P2RX7, NEK7, NLRP3, TNF and RIPK3 in DSS-treated mice after BXD intervention (Table 3). These findings further suggested that BXD ameliorates UC through the modulation of pyroptosis and necroptosis. As reported in the literature, P2RX7-mediated potassium efflux facilitates the interaction between NEK7 and NLRP3, promoting pyroptosis.[25] The involvement of the TNF receptor TNFR1 and RIPK3 is a characteristic of necroptosis activation.[26] Therefore, it is hypothesized that the P2RX7/NEK7 and TNFR1/RIPK3 signaling pathways play key roles in UC mice treated with BXD.

BXD Inhibited Pyroptosis and Necroptosis in DSS Mice via the P2RX7/NEK7 and TNFR1/RIPK3 Pathways

This study further explored the role of pyroptosis and necroptosis in DSS-induced mice, and investigated the multi-pathway mechanism through which BXD exerts its effects. GSDMD-N and p-MLKL were utilized as specific markers for NLRP3 inflammasome-mediated pyroptosis and RIPK3-mediated necroptosis, respectively. Immunohistochemistry staining showed that DSS induced the upregulation of GSDMD-N and p-MLKL, indicating the activation of pyroptosis and necroptosis in the intestines of DSS mice. Notably, BXD treatment effectively attenuated these increases, as evidenced by the reduced protein levels of GSDMD-N and p-MLKL in the colon (Figure 6A and B). Western blot analysis showed that BXD treatment significantly suppressed the colonic protein expression of P2RX7, NEK7, NLRP3, ASC, and cleaved IL-1β. Moreover, BXD treatment decreased the ratios of cleaved caspase-1 to caspase-1 and GSDMD-N to GSDMD in DSS-treated mice (Figure 6C and D). Furthermore, in comparison to DSS treatment, BXD treatment resulted in a downregulation of TNFR1 protein expression and a reduction in the phosphorylation levels of RIPK1, RIPK3, and MLKL (Figure 6E and F). Collectively, these data demonstrated that UC induces both pyroptosis and necroptosis in colon tissues, which are effectively suppressed by BXD through concurrent inhibition of the P2RX7/NEK7 and TNFR1/RIPK3 pathways.

BXD Protects Against LPS+TNF-α Induced Pyroptosis and Necroptosis in NCM460 Cells

To further confirm the protective effects of BXD, pyroptosis and necroptosis were induced in NCM460 cells under model conditions using a combination of 1 μg/mL LPS, 100 ng/mL TNF-α, and 20 μM nigericin. BXD was then administered at nontoxic concentrations (3.125, 6.25, and 12.5 μg/mL) for intervention (Figure 7A). Microscopic analysis showed that control NCM460 cells had intact plasma membranes with preserved structural integrity. In contrast, LPS+TNF-α-induced cells exhibited pyroptotic and necroptotic features, such as significant swelling and membrane rupture. Notably, BXD at concentrations of 6.25 and 12.5 μg/mL effectively inhibited LPS+TNF-α-triggered pyroptosis and necroptosis

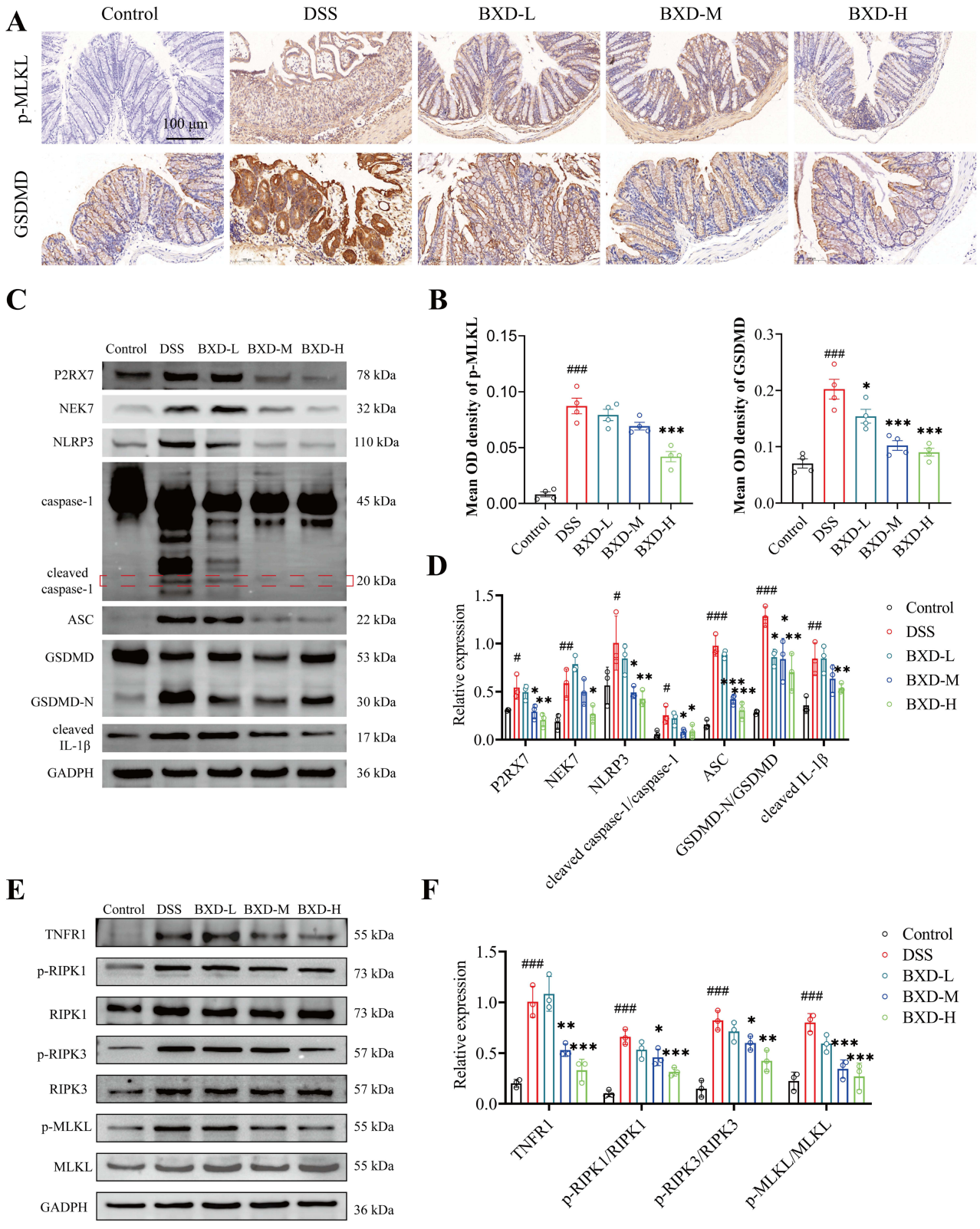

Figure 6 BXD reversed pyroptosis and necroptosis via the P2RX7/NEK7 and TNFR1/RIPK3 pathways in DSS mice. (**A**) IHC results of p-MLKL and GSDMD expression. (**B**) Mean OD density of p-MLKL and GSDMD immunostaining (n=4). (**C** and **D**) Western blot analysis of colonic P2RX7, NEK7, NLRP3, caspase-1, cleaved caspase-1, ASC, GSDMD, GSDMD-N and cleaved IL-1β (n=3). (**E** and **F**) Western blot analysis of colonic TNFR1, p-RIPK1, RIPK1, p-RIPK3, RIPK3, p-MLKL and MLKL (n=3). Data were presented as mean±SEM. $^{\#\#\#\#}P < 0.001$, $^{\#\#\#}P < 0.01$, $^{\#}P < 0.05$ vs control group; $^{***}P < 0.001$, $^{**}P < 0.01$, $^{*}P < 0.05$ vs DSS group.

(Figure 7B). The LDH assay further validated the protective effect of BXD against PCD (Figure 7C). Additionally, in a concentration-dependent way, BXD treatment significantly reduced the upregulation of IL-1β and HMGB1 in the cell supernatants (Figure 7D). The Annexin V-FITC/PI assay confirmed that LPS+TNF-α stimulation markedly elevated the proportion of cell death (57.59%, defined as the sum of the Q2 and Q3 populations) relative to the control group (3.01%). BXD at 12.5 μg/mL reduced the number of Q2 and Q3 cells (21.65%), effectively reversing LPS+TNF-α-induced cell death (Figure 7E and F). Immunofluorescence showed that the LPS+TNF-α-induced upregulation of GSDMD-N and p-MLKL was attenuated by BXD treatment (Figure 7G and H). Western blot analysis further confirmed that BXD significantly downregulated the protein expression of the P2RX7/NEK7 and TNFR1/RIPK3 pathways in LPS+TNF-α-stimulated NCM460 cells (Figure 8A–D). These findings underscored the function of BXD in suppressing pyroptosis and necroptosis in intestinal epithelial cells, further corroborating its protective effects.

Verification of Potential Pharmacodynamic Substances of BXD

Using LDH release and IL-1β levels as screening criteria, 23 candidate compounds derived from BXD were selected for subsequent validation. As shown in Figure 9A, LPS+TNF-α exposure for 24 h significantly increased LDH release relative to the control group. In contrast, treatment with baicalin, scutellarin, glycyrrhizic acid or glycyrrhetinic acid

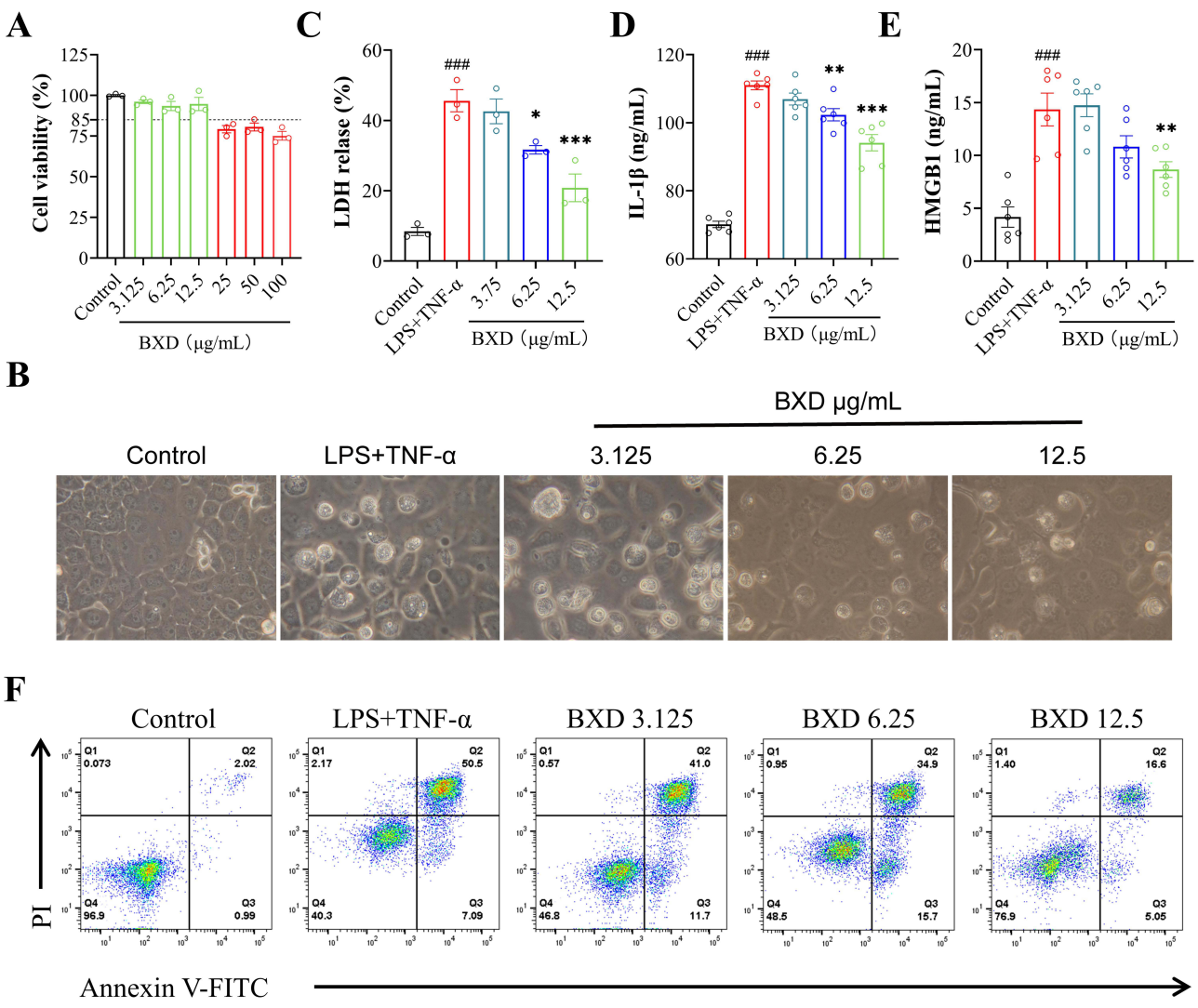

Figure 7 Continued.

https://doi.org/10.2147/JIR.S564333

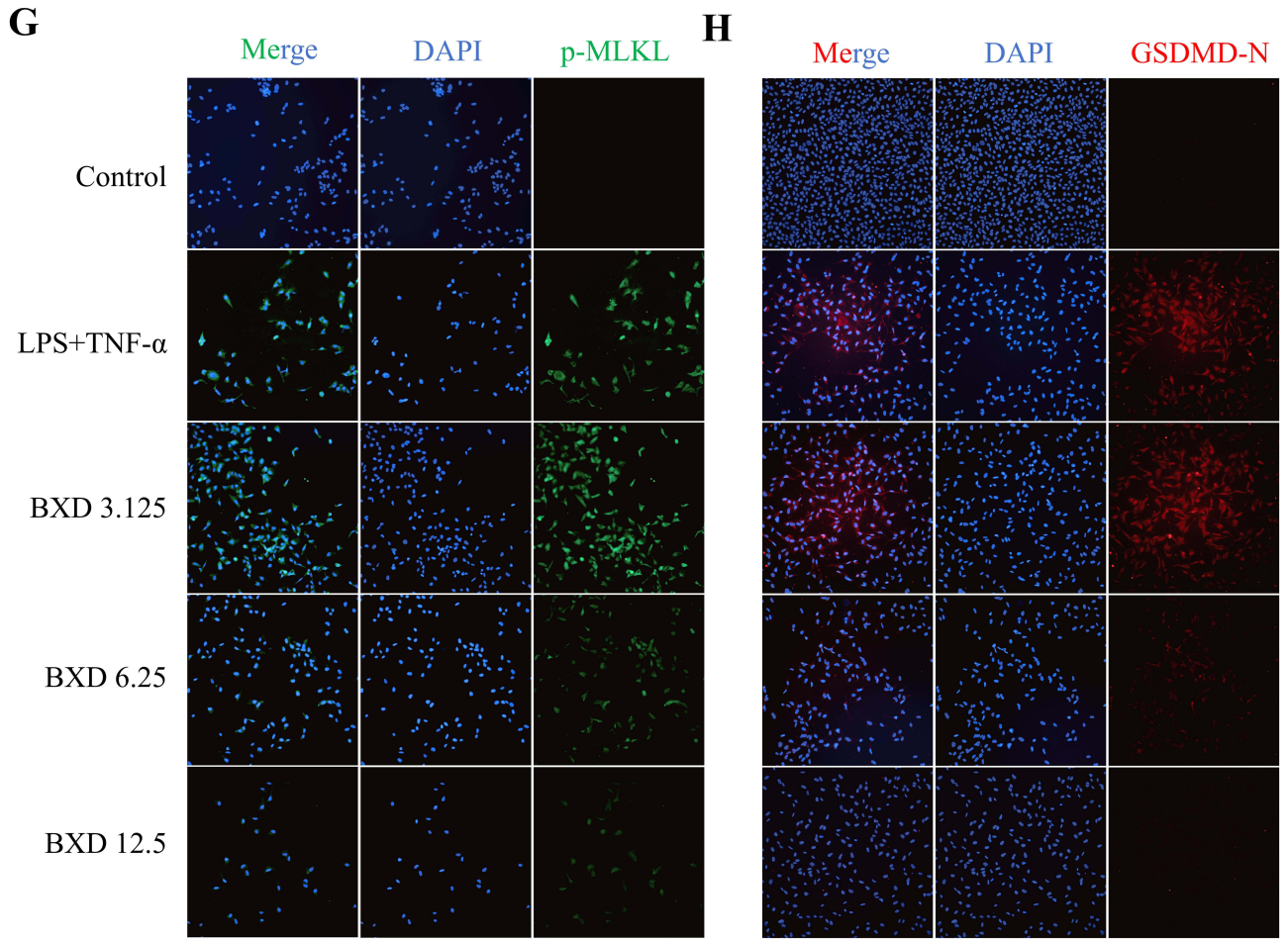

Figure 7 Effects of BXD on pyroptosis and necroptosis in NCM460 cells stimulated by LPS+TNF-α. (**A**) Cytotoxicity assay of BXD in NCM460 cells treated with 3.125, 6.25, or 12.5 μg/mL BXD for 24 h. (**B**) Microscopy images of NCM460 cells pretreated with different concentrations of BXD for 8 h followed by LPS+TNF-α stimulation for another 24 h. (**C**–**E**) LDH release assay and ELISA detection of IL-1β and HMGB1 in the cell supernatants. (**F**) Cell death analysis by Annexin V-FITC/PI staining in LPS+TNF-α-induced NCM460 cells after different treatments (magnification, 100×). (**G** and **H**) Immunofluorescence staining of GSDMD-N and p-MLKL in the NCM460 cell model. Data were presented as mean±SEM (n=3). $^{\#\#\#}P < 0.001$ vs control group; $^{***}P < 0.001$, $^{**}P < 0.01$, $^{*}P < 0.05$ vs LPS+TNF-α group.

markedly reduced LDH release, indicating their potential to alleviate cell death. Furthermore, among the tested active constituents, baicalin, scutellarin, oroxylin A, berberine, coptisine, glycyrrhizic acid, and glycyrrhetinic acid inhibited IL-1β secretion in the cell supernatants (Figure 9B).

Identification of Components from BXD That Target the P2RX7/NEK7 and TNFR1/RIPK3 Pathways

As mentioned above, the P2RX7/NEK7 and TNFR1/RIPK3 signaling pathways play critical roles alleviating UC in BXD, as concluded from comprehensive multi-omics analysis and in vitro and in vivo validation. The core targets P2RX7 and TNFR1, along with 23 potential active compounds in BXD, were selected for molecular docking to assess protein-ligand binding affinity.

The molecular docking results for 23 compounds in BXD with P2RX7 and TNFR1 target proteins are presented in Figure 10A. It is widely recognized that lower binding energies signify more stable receptor-ligand interactions. The results showed that 21 compounds in BXD could interact with the docking pockets of P2RX7 and TNFR1, except for ginsenoside Rb1 and 6-gingerol. Specifically, baicalin, berberine, coptisine, epiberberine, scutellarin, and isoliquiritin presented greater binding affinities for P2RX7 than did the positive control A839977 (−9.0 kcal/mol). Baicalein,

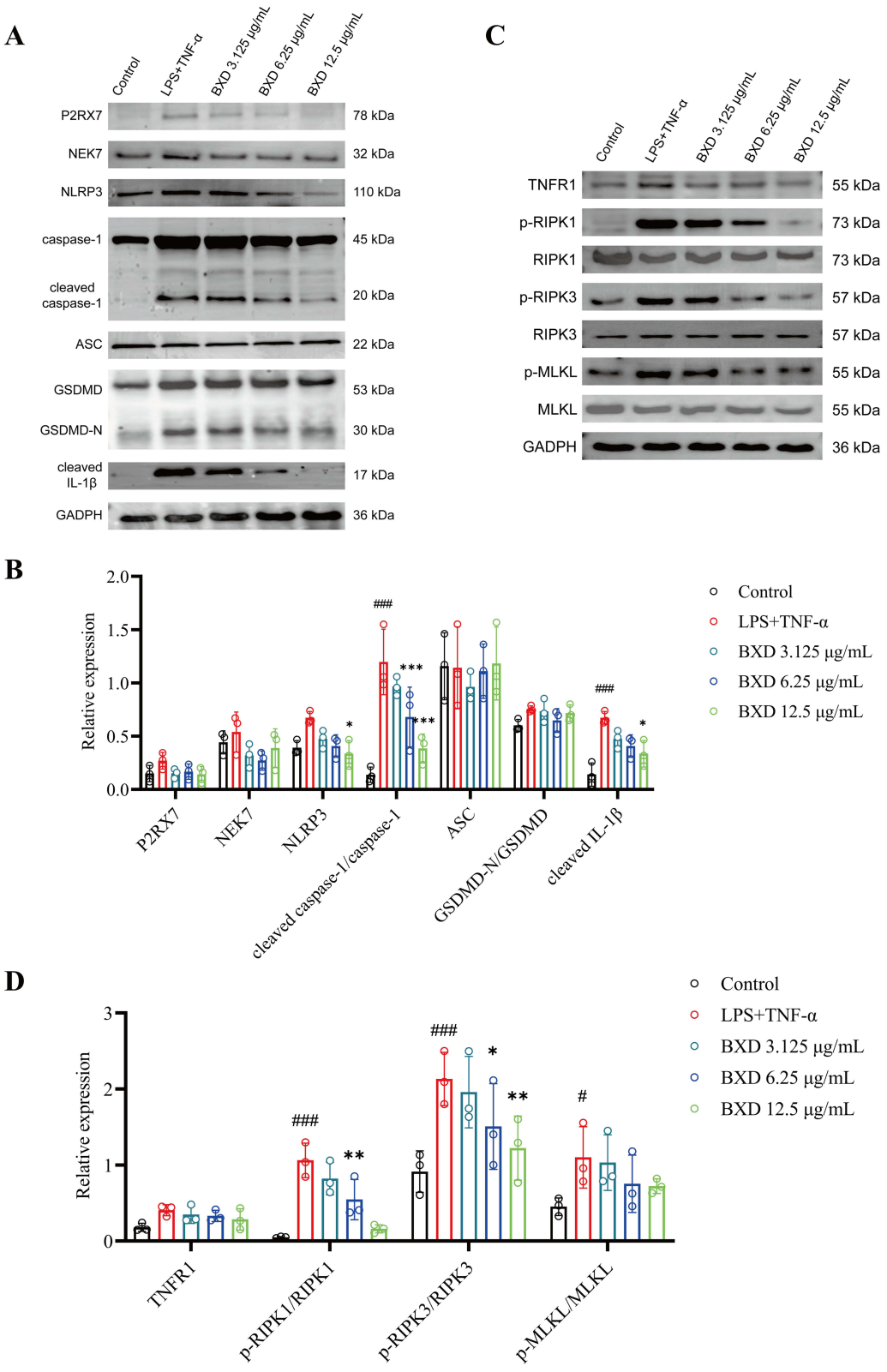

Figure 8 BXD inhibited pyroptosis and necroptosis via the P2RX7/NEK7 and TNFR1/RIPK3 pathways in NCM460 cells. (**A** and **B**) Western blot analysis of P2RX7, NEK7, NLRP3, caspase-1, cleaved caspase-1, ASC, GSDMD, GSDMD-N, and cleaved IL-1β (**C** and **D**) Western blot analysis of TNFR1, p-RIPK1, RIPK1, p-RIPK3, RIPK3, p-MLKL and MLKL. Data were presented as mean±SEM (n=3). $^{###}P < 0.001$, $^{#}P < 0.05$ vs control group; $^{***}P < 0.001$, $^{**}P < 0.01$, $^{*}P < 0.05$ vs LPS+TNF-α group.

https://doi.org/10.2147/JIR.S564333

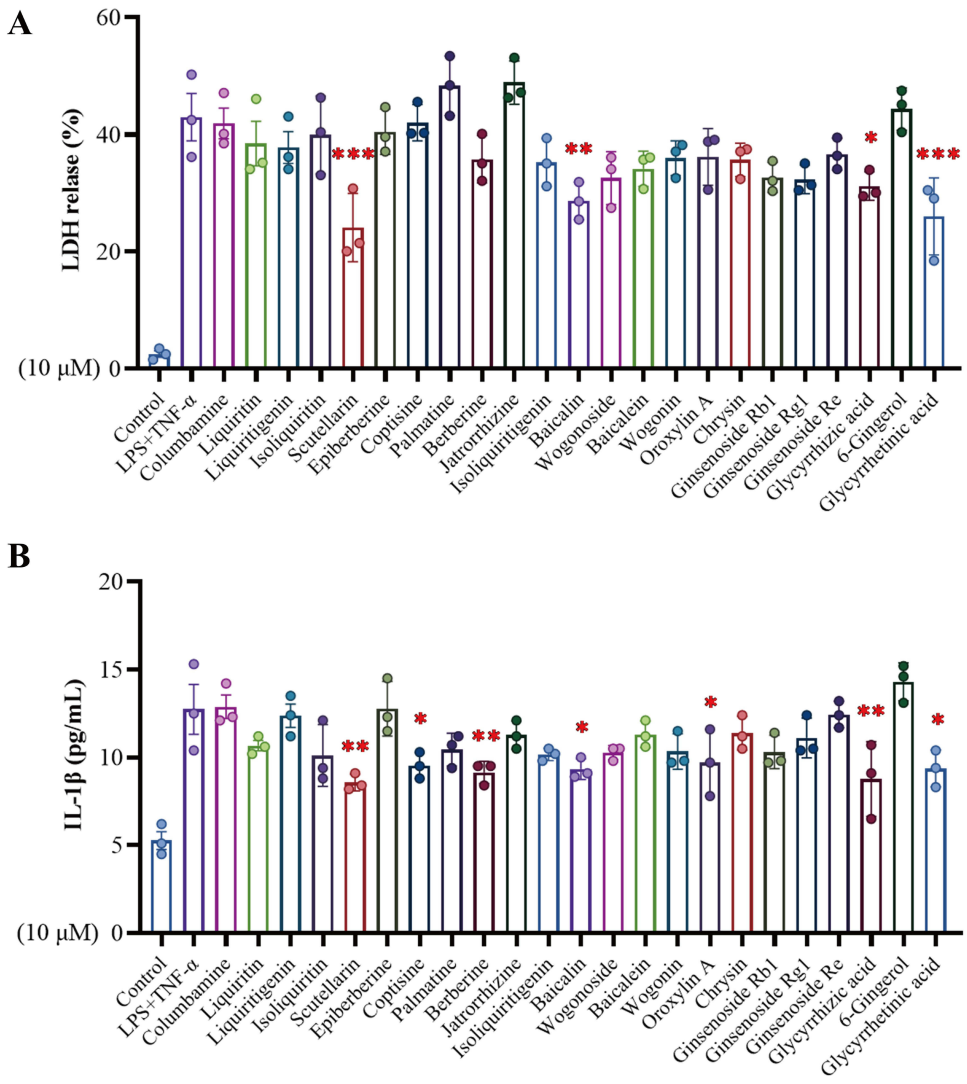

Figure 9 Protective effects of components of BXD against pyroptosis and necroptosis. (**A**) LDH release assay. The cells were treated with 10 μM for 8 h. (**B**) ELISA detection of IL-1β secretion in NCM460 cells. Data were presented as mean±SEM (n=3). ***$P < 0.001$, **$P < 0.01$, *$P < 0.05$ vs LPS+TNF-α group.

berberine, chrysin, coptisine, glycyrrhizic acid, isoliquiritin, and liquiritigenin had greater binding affinity for TNFR1 than did the positive control balinatunfib (−6.4 kcal/mol).

To enhance the validation of the docking results, SPR analysis was performed to evaluate the binding affinities of the top five compounds chosen according to their binding energy scores. The results showed that baicalin, berberine, coptisine, epiberberine, and scutellarin exhibited specific binding to P2RX7, with baicalin demonstrating the lowest kinetic fitting parameter (KD = 0.6912 μM), indicating a high-affinity interaction (Figure 10B and D). Moreover, berberine, coptisine and glycyrrhizic acid exhibited specific binding to TNFR1, with glycyrrhizic acid demonstrating the lowest kinetic fitting parameter (KD = 57.35 μM), indicating a medium-affinity interaction (Figure 10C and E). Figure 10F visually illustrated the protein-ligand interaction profiles of baicalin with P2RX7 and glycyrrhizic acid with TNFR1. Baicalin has a similar binding interaction to A839977 with P2RX7, forming hydrogen bonds with residues LYS-110, ILE-310, THR-94, TRP-167, TYR-298, PHE-88, and SER-149. Compared with balinatunfib, glycyrrhizic acid partially differs in its binding interaction with TNFR1, marked by the hydrogen bond formation with residues ALA-62, ASP-91, LYS-132, and LYS-35. Collectively, these observations indicate that the impact of BXD on pyroptosis and necroptosis may be mediated by its active components. Specifically, baicalin may interact with P2RX7, and glycyrrhizic acid may target TNFR1.

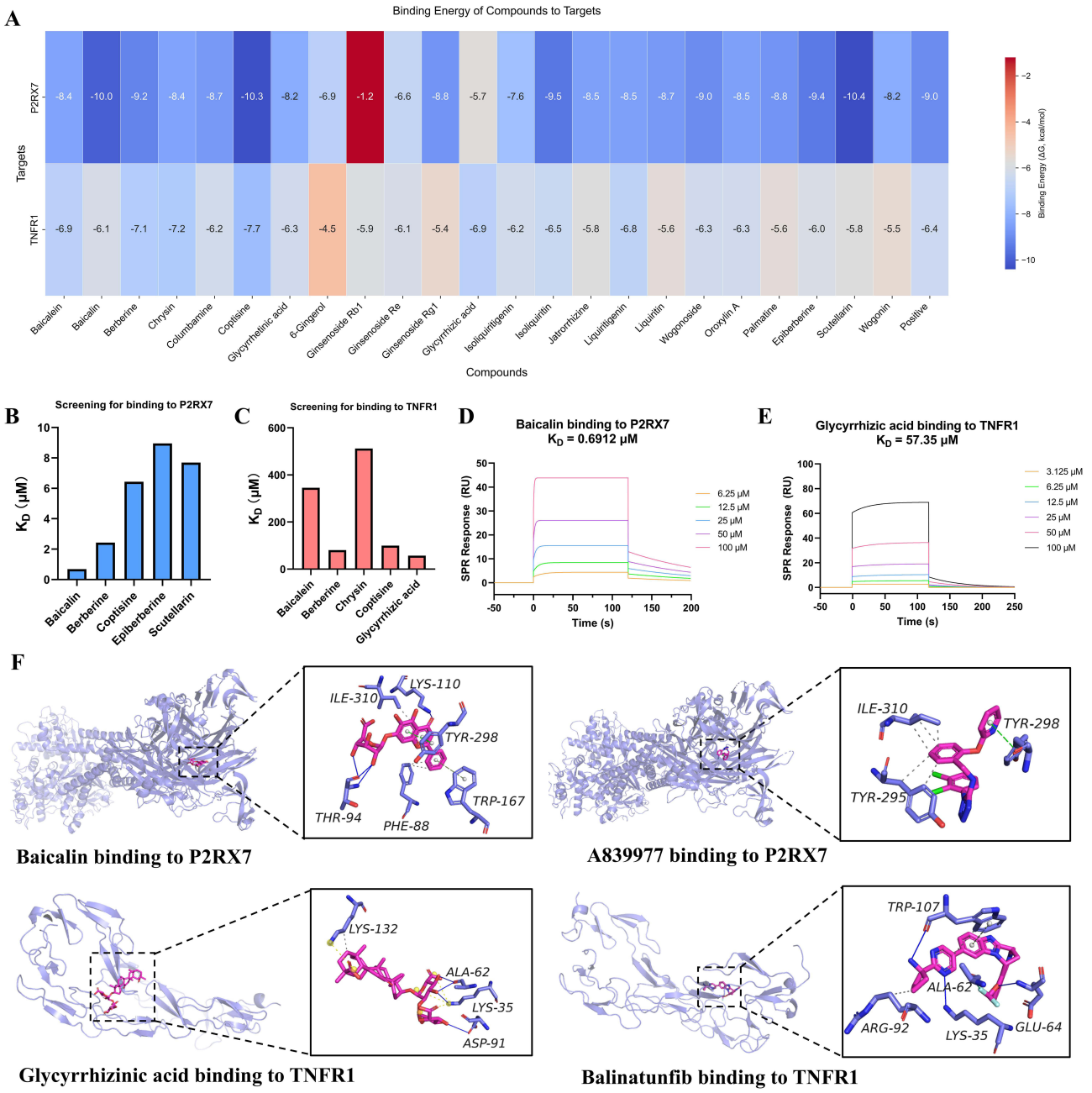

Figure 10 Molecular docking and SPR screening of BXD bioactive components targeting P2RX7 and TNFR1. (**A**) Molecular docking analysis of the bioactive components in BXD with P2RX7 and TNFR1 target proteins. The positive controls A839977 and balinatunfib were included for comparison. (**B** and **C**) SPR screening of the top five BXD compounds that bind to P2RX7 and TNFR1. (**D** and **E**) SPR analysis of Baicalin binding to P2RX7 and glycyrrhizic acid binding to TNFR1. (**F**) Visual representation of the protein-ligand interaction profiles between baicalin, A839977 and P2RX7, as well as between glycyrrhizic acid, balinatunfib and TNFR1.

Discussion

UC is a common autoimmune disease, and its etiology is associated with multiple factors such as genetics, immune disorders, and intestinal flora imbalance. Mounting evidence indicates that PCD is pivotal to the occurrence and progression of UC, especially pyroptosis and necroptosis.[27,28] Several natural compounds targeting pyroptosis and necroptosis have shown potential therapeutic effects against UC, indicating that these two forms of PCD serve as key targets for UC treatment.[29,30]

BXD is commonly incorporated into Chinese herbal compounds for the management of UC, and modern pharmacological studies confirm its therapeutic efficacy.[31] The present study revealed that BXD significantly ameliorated DSS

https://doi.org/10.2147/JIR.S564333

symptoms, reversed both local and systemic inflammatory pathology, preserved intestinal barrier function, and reduced cell death. Considering that epithelial barrier disruption and inflammation are central features of UC and that recent studies implicate PCD in UC progression,[32] our findings indicate that the protective effects of BXD are intricately associated with the regulation of cell death.

Transcriptomic analysis revealed enrichment of the NOD-like receptor signaling pathway, the IL-17 signaling pathway, and the TNF signaling pathway following BXD treatment. Similarly, proteomic analysis revealed that BXD regulated the NOD-like receptor signaling pathway, cytosolic DNA-sensing pathway, and C-type lectin receptor signaling pathway. These pathways are strongly implicated in the inflammatory response in UC and may regulate PCD.[33] Importantly, both the transcriptomic and proteomic data consistently highlighted the NOD-like receptor pathway. BXD markedly downregulated the expression of key proteins or genes, including TNF, RIPK3, P2RX7, NEK7, and NLRP3, implicating PCD regulation as a major mechanism. These observations support the hypothesis that excessive pyroptosis and necroptosis represent important mechanisms of UC,[34] and BXD exerts its effects by inhibiting pyroptosis and necroptosis.

The role of pyroptosis and necroptosis in the pathophysiology of UC has garnered significant interest in recent years, with ongoing discoveries on their regulatory mechanisms. Mechanistically, P2RX7 functions as the cellular stress sensor molecule and initiates inflammasome activation.[35] Upon cellular injury, extracellular ATP levels increase and bind to P2RX7, triggering K^+ efflux. Subsequent to this K^+ efflux signal, NEK7 is recruited to interact with NLRP3, resulting in the formation of the NLRP3 inflammasome complex. The inflammasome complex promotes the cleavage of caspase-1 and GSDMD, resulting in the secretion of IL-1β and pyroptosis.[36,37] Excessive pyroptosis, driven by aberrant P2RX7 activation, markedly exacerbates colonic tissue damage and disrupts epithelial barrier integrity.[38] In DSS-established colitis models, the expression levels of P2RX7 and GSDMD-N were significantly upregulated. These changes indicate that P2RX7 activation occurs in this model, accompanied by the process of pyroptosis. Consistent with previous reports that P2RX7 inhibition alleviates experimental colitis,[39,40] the results of our study suggest that BXD reduced the protein expression of P2RX7 and NEK7, suppressed NLRP3 inflammasome activation, thereby preventing pyroptosis in DSS mice.

The role of TNFR1 in necroptosis is critical. TNFR1 is a transmembrane receptor that functions as the primary signal transduction center for TNF-α. TNF-α triggers necroptosis by activating downstream signaling pathways through TNFR1, and phosphorylating RIPK1, RIPK3, and MLKL.[8] Research has shown that necroptosis-related proteins are upregulated in UC patients,[41] and that pharmacological inhibition of this pathway mitigates UC.[42] Although no TNFR1-targeted drugs have been approved to date, current clinical trials have demonstrated the effective role of TNFR1 inhibitor in UC.[43] Western blotting and immunocytochemistry showed a significant increase in MLKL phosphorylation, suggesting the presence of necroptosis in colonic tissues. After DSS-treated mice received BXD treatment, the expression levels of TNFR1 and necroptosis-related proteins phosphorylation were significantly decreased, indicating that BXD may inhibit necroptosis via the TNFR1/RIPK3 pathway. Concurrently, we observed reduced protein and mRNA levels of TNF-α in colon tissue. This further demonstrates that BXD can inhibit both the aforementioned factor and its corresponding receptor. In vitro experiments, we used LPS, TNF-α and Nigericin to induce pyroptosis and necroptosis in intestinal epithelial cells. The results showed that BXD reduced the release of inflammatory cytokines and LDH, as well as the ratio of Annexin V/PI-positive cells, which indicate that BXD had excellent anti-PCD activities on intestinal epithelial cells. Western blotting and immunofluorescence further showed that BXD inhibited the NLRP3 inflammasome-medicated pyroptosis through the P2RX7/NEK7 pathway, and necroptosis via the TNFR1/RIPK3 pathway in intestinal epithelial cells. It is worth noting that other pharmacological compounds can also ameliorate DSS-induced colitis models, achieved by the simultaneous suppression of pyroptosis and necroptosis.[44] Together, these findings point to the fact that BXD exerts synergistic anti-colitic effects by inhibiting pyroptosis and necroptosis.

Furthermore, screening of BXD components revealed that flavonoids and triterpenoid saponins, particularly baicalin and glycyrrhizic acid, effectively significantly decreased LDH release and the IL-1β level. In contrast, alkaloids, particularly berberine, have no obvious ability to resist cell death but can reduce the concentration of IL-1β. Molecular docking analyses revealed that all the tested components, with the exception of 6-gingerol, ginsenoside Rb1, ginsenoside Re1, and glycyrrhizic acid, displayed favorable binding energies to P2RX7, which were comparable to

those of the P2RX7 inhibitor A839977. Baicalein, berberine, chrysin, coptisine, glycyrrhizic acid, isoliquiritin, and liquiritigenin exhibited favorable binding energies to TNFR1, which were comparable to those of the TNFR1 inhibitor balinatunfib. SPR analysis further characterized the molecular interactions between baicalin and P2RX7, as well as between glycyrrhizic acid and TNFR1. These results identify baicalin and glycyrrhizic acid as major active constituents that act on distinct but complementary targets, providing a mechanistic explanation for the multi-component synergy of BXD.

Nevertheless, the independent contributions of baicalin and glycyrrhizic acid have yet to be fully characterized. Future research should systematically evaluate their in vivo and in vitro effects, particularly regarding the P2RX7/NEK7 and TNFR1/RIPK3 pathways, to clarify additive versus synergistic effects. In clinical practice, IBD treatment often requires combined therapies to achieve synergistic effects. Future research could investigate the combination of BXD with conventional drugs (aminosalicylates, glucocorticoids, or biological agents) to evaluate whether this approach can enhance therapeutic efficacy, reduce drug dosage, and minimize adverse reactions. Additionally, the combination of BXD

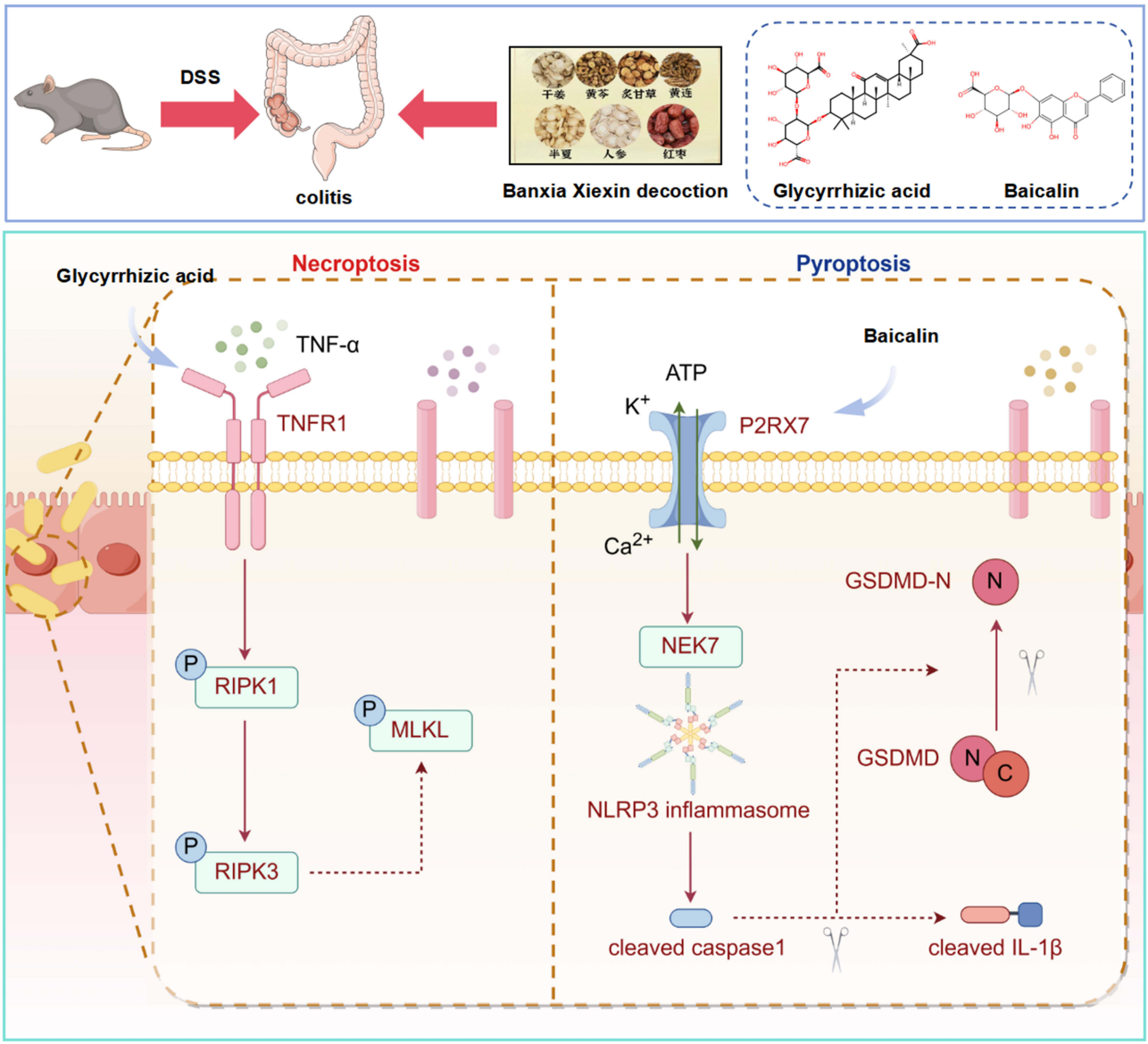

Figure 11 Molecular mechanism diagram. Banxia Xiexin decoction reduces pyroptosis and necroptosis by inhibiting the P2RX7/NEK7 and TNFR1/RIPK3 signaling.

https://doi.org/10.2147/JIR.S564333

with dietary interventions or probiotics may provide a more comprehensive strategy for managing IBD, given the close interplay between gut microbiota and intestinal inflammation.

In conclusion, BXD ameliorates UC through dual inhibition of pyroptosis and necroptosis. Specifically, BXD downregulates P2RX7 and blocks NLRP3 inflammasome activation to suppress pyroptosis, while simultaneously reducing TNFR1 expression and RIPK1/RIPK3-mediated signaling to inhibit necroptosis. Baicalin and glycyrrhizic acid are key pharmacodynamic constituents that target P2RX7 and TNFR1, respectively, and their complementary actions likely underlie the therapeutic synergy of BXD. The proposed mechanism by which BXD exerts its effects in UC is summarized in Figure 11.

Conclusion

BXD exerts a protective effect against DSS-induced colitis in mice by alleviating inflammation and intestinal barrier impairment. Mechanistically, BXD inhibits NLRP3 inflammasome-mediated pyroptosis via the P2X7R/NEK7 pathway and necroptosis by suppressing the TNFR1/RIPK3 pathway. Baicalin and glycyrrhizic acid are key bioactive components of BXD to reduce pyroptosis and necroptosis, respectively. These findings clarify the molecular and material foundation of BXD, emphasizing the promise of traditional herbal formulae for UC.

Abbreviations

AB, alcian blue; BXD, Banxia Xiexin decoction; CCK-8, Cell Counting Kit-8; DAI, disease activity index; DEGs, differentially expressed genes; DEPs, differentially expressed proteins; DSS, dextran sulfate sodium salt; H&E, hematoxylin and eosin; IL, interleukin; LPS, lipopolysaccharide; MPO, myeloperoxidase; PAS, periodic acid Schiff; PBS, phosphate buffer saline; PCA, principle component analysis; PCD, programmed cell death; PPI, protein-protein interaction; TNF, tumor necrosis factor; UC, ulcerative colitis; TCM, traditional Chinese medicine; TUNEL, TdT mediated dUTP nick end labeling; LDH, lactate dehydrogenase; SPR, surface Plasmon Resonance; KEGG, Kyoto encyclopedia of genes and genomes.

Data Sharing Statement

Data will be made available on request from the corresponding author [Xinhong Wang].

Author Contributions

Jie Lu: Investigation, Data curation, Methodology, Writing-original draft. Kun Liang: Methodology, Software, Writing-original draft. Li Zhang: Supervision, Formal analysis. Bo Cui: Formal analysis. Lisha You: Methodology. Rui An: Funding acquisition, Supervision, Methodology, Conceptualization. Cheng Hu: Supervision, Conceptualization. Xinhong Wang: Conceptualization, Funding acquisition, Supervision. All authors participated in drafting, revising, or critically reviewing the article, approved the final version to be published, reached a consensus on the journal to which the article was submitted, and agreed to be accountable for all aspects of the research work.

Funding

This study received funding from the National Natural Science Foundation of China (Grant No. 82274446 and 8237152155).

Disclosure

All authors declared no relevant conflicts of interest.

References

1. Chang JT. Pathophysiology of inflammatory bowel diseases. *N Engl J Med*. 2020;383(27):2652–2664. doi:10.1056/NEJMra2002697
2. Kobayashi T, Siegmund B, Le Berre C, et al. Ulcerative colitis. *Nat Rev Dis Primers*. 2020;6(1):74. doi:10.1038/s41572-020-0205-x
3. Belkaid Y, Hand TW. Role of the microbiota in immunity and inflammation. *Cell*. 2014;157(1):121–141. doi:10.1016/j.cell.2014.03.011

4. Chao L, Zhang W, Feng Y, Gao P, Ma J. Pyroptosis: a new insight into intestinal inflammation and cancer. *Front Immunol*. 2024;15:1364911. doi:10.3389/fimmu.2024.1364911
5. Patankar JV, Becker C. Cell death in the gut epithelium and implications for chronic inflammation. *Nat Rev Gastroenterol Hepatol*. 2020;17(9):543–556. doi:10.1038/s41575-020-0326-4
6. Wang JM, Yang J, Xia WY, et al. Comprehensive analysis of PANoptosis-related gene signature of ulcerative colitis. *Int J Mol Sci*. 2023;25(1):348. doi:10.3390/ijms25010348
7. Rao Z, Zhu Y, Yang P, et al. Pyroptosis in inflammatory diseases and cancer. *Theranostics*. 2022;12(9):4310–4329. doi:10.7150/thno.71086
8. Akanyibah FA, Zhu Y, Jin T, Ocansey DKW, Mao F, Qiu W. The function of necroptosis and its treatment target in IBD. *Mediators Inflamm*. 2024;2024:7275309. doi:10.1155/2024/7275309
9. Ye Z, Deng M, Yang Y, et al. Epithelial mitochondrial fission-mediated PANoptosis is crucial for ulcerative colitis and its inhibition by saquinavir through Drp1. *Pharmacol Res*. 2024;210:107538. doi:10.1016/j.phrs.2024.107538
10. Yang L, Liu X, Zhu J, et al. Progress in traditional Chinese medicine against chronic gastritis: from chronic non-atrophic gastritis to gastric precancerous lesions. *Heliyon*. 2023;9(6):e16764. doi:10.1016/j.heliyon.2023.e16764
11. Wang QR, Shao J. Chinese medicinal formulae treat inflammatory bowel diseases through maintaining gut flora homeostasis. *Zhongguo Zhong Yao Za Zhi*. 2022;47(22):5997–6004. doi:10.19540/j.cnki.cjcmm.20220706.501
12. Yuan S, Wang N, Wang JL, et al. Gender differences in damp-heat syndrome: a review. *Biomed Pharmacother*. 2021;143:112128. doi:10.1016/j.biopha.2021.112128
13. Zhang B, Liu K, Yang H, Jin Z, Ding Q, Zhao L. Gut microbiota: the potential key target of TCM's therapeutic effect of treating different diseases using the same method-UC and T2DM as examples. *Front Cell Infect Microbiol*. 2022;12:855075. doi:10.3389/fcimb.2022.855075
14. Sin SH, Wu J, Kang Y, et al. Efficacy of modified Banxia Xiexin decoction in the management of Wei-Pi syndrome (postprandial distress syndrome): study protocol for a randomized, waitlist-controlled trial. *Trials*. 2021;22(1):135. doi:10.1186/s13063-021-05078-y
15. Chen G, Yang Y, Liu M, et al. Banxia xiexin decoction protects against dextran sulfate sodium-induced chronic ulcerative colitis in mice. *J Ethnopharmacol*. 2015;166:149–156. doi:10.1016/j.jep.2015.03.027
16. Cui T, Yue Y, Yan S. Current evidence for Banxia Xiexin decoction in gastrointestinal tumors and future research perspectives. *J Ethnopharmacol*. 2025;351:119972. doi:10.1016/j.jep.2025.119972
17. Luo Y, Fu S, Liu Y, et al. Banxia Xiexin decoction modulates gut microbiota and gut microbiota metabolism to alleviate DSS-induced ulcerative colitis. *J Ethnopharmacol*. 2024;326:117990. doi:10.1016/j.jep.2024.117990
18. Zhou Z, An R, You L, Liang K, Wang X. Banxia Xiexin decoction: a review on phytochemical, pharmacological, clinical and pharmacokinetic investigations. *Medicine*. 2023;102(35):e34891. doi:10.1097/md.0000000000034891
19. Wang W, Gu W, He C, Zhang T, Shen Y, Pu Y. Bioactive components of Banxia Xiexin Decoction for the treatment of gastrointestinal diseases based on flavor-oriented analysis. *J Ethnopharmacol*. 2022;291:115085. doi:10.1016/j.jep.2022.115085
20. Dunleavy KA, Raffals LE, Camilleri M. Intestinal barrier dysfunction in inflammatory bowel disease: underpinning pathogenesis and therapeutics. *Dig Dis Sci*. 2023;68(12):4306–4320. doi:10.1007/s10620-023-08122-w
21. Wirtz S, Popp V, Kindermann M, et al. Chemically induced mouse models of acute and chronic intestinal inflammation. *Nat Protoc*. 2017;12(7):1295–1309. doi:10.1038/nprot.2017.044
22. Li X, Zhang M, Huang X, et al. Ubiquitination of RIPK1 regulates its activation mediated by TNFR1 and TLRs signaling in distinct manners. *Nat Commun*. 2020;11(1):6364. doi:10.1038/s41467-020-19935-y
23. Lee S, Karki R, Wang Y, Nguyen LN, Kalathur RC, Kanneganti TD. AIM2 forms a complex with pyrin and ZBP1 to drive PANoptosis and host defence. *Nature*. 2021;597(7876):415–419. doi:10.1038/s41586-021-03875-8
24. Wanli AJ, Zehua AZ, Tingting AW, Rui AA, Kun AL, Xinhong AW. Analysis of chemical constituents in banxia xiexin decoction based on UPLC-LTQ-Orbitrap-MS method. *Chin J Pharmaceut Anal*. 2020;40(10):1736–1750. doi:10.16155/j.0254-1793.2020.10.03
25. Di Virgilio F, Dal Ben D, Sarti AC, Giuliani AL, Falzoni S. The P2X7 receptor in infection and inflammation. *Immunity*. 2017;47(1):15–31. doi:10.1016/j.immuni.2017.06.020
26. Dondelinger Y, Darding M, Bertrand MJ, Walczak H. Poly-ubiquitination in TNFR1-mediated necroptosis. *Cell Mol Life Sci*. 2016;73(11–12):2165–2176. doi:10.1007/s00018-016-2191-4
27. Burdette BE, Esparza AN, Zhu H, Wang S. Gasdermin D in pyroptosis. *Acta Pharm Sin B*. 2021;11(9):2768–2782. doi:10.1016/j.apsb.2021.02.006
28. Liu C, Wang H, Han L, et al. Targeting P2Y(14)R protects against necroptosis of intestinal epithelial cells through PKA/CREB/RIPK1 axis in ulcerative colitis. *Nat Commun*. 2024;15(1):2083. doi:10.1038/s41467-024-46365-x
29. Alagbaoso CA, Mizuno M. Polysaccharides from Shiitake culinary-medicinal mushroom Lentinus edodes (Agaricomycetes) suppress pMLKL-mediated necroptotic cell death and colitis in mice. *Int J Med Mushrooms*. 2021;23(7):13–26. doi:10.1615/IntJMedMushrooms.2021038850
30. Liu X, Zhou M, Dai Z, et al. Salidroside alleviates ulcerative colitis via inhibiting macrophage pyroptosis and repairing the dysbacteriosis-associated Th17/Treg imbalance. *Phytother Res*. 2023;37(2):367–382. doi:10.1002/ptr.7636
31. Ji W, Liu W, Huo Y, Hu C, Zhang Y. Banxia Xiexin decoction ameliorates dextran sulfate sodium (DSS)-induced ulcerative colitis via inhibiting serine-threonine protein kinase (Akt)/mitogen-activated protein kinase (MAPK) signaling pathway. *Biotechnol Appl Biochem*. 2023;70(4):1530–1542. doi:10.1002/bab.2451
32. Nakase H, Sato N, Mizuno N, Ikawa Y. The influence of cytokines on the complex pathology of ulcerative colitis. *Autoimmun Rev*. 2022;21(3):103017. doi:10.1016/j.autrev.2021.103017
33. Li D, Wu M. Pattern recognition receptors in health and diseases. *Signal Transduct Target Ther*. 2021;6(1):291. doi:10.1038/s41392-021-00687-0
34. Sharma D, Kanneganti TD. Inflammatory cell death in intestinal pathologies. *Immunol Rev*. 2017;280(1):57–73. doi:10.1111/imr.12602
35. Pelegrin P. P2X7 receptor and the NLRP3 inflammasome: partners in crime. *Biochem Pharmacol*. 2021;187:114385. doi:10.1016/j.bcp.2020.114385
36. Xia J, Jiang S, Dong S, Liao Y, Zhou Y. The role of post-translational modifications in regulation of NLRP3 inflammasome activation. *Int J Mol Sci*. 2023;24(7):6126. doi:10.3390/ijms24076126
37. Zhan X, Li Q, Xu G, Xiao X, Bai Z. The mechanism of NLRP3 inflammasome activation and its pharmacological inhibitors. *Front Immunol*. 2022;13:1109938. doi:10.3389/fimmu.2022.1109938

38. Song Y, Ma Y, Zhao Y, et al. Biological functions of NLRP3 inflammasome: a therapeutic target in inflammatory bowel disease. *Cytokine Growth Factor Rev*. 2021;60:61–75. doi:10.1016/j.cytogfr.2021.03.003
39. Jin X, Liu D, Zhou X, Luo X, Huang Q, Huang Y. Entrectinib inhibits NLRP3 inflammasome and inflammatory diseases by directly targeting NEK7. *Cell Rep Med*. 2023;4(12):101310. doi:10.1016/j.xcrm.2023.101310
40. Abad C, Demeules M, Guillou C, et al. Administration of an AAV vector coding for a P2X7-blocking nanobody-based biologic ameliorates colitis in mice. *J Nanobiotechnol*. 2024;22(1):27. doi:10.1186/s12951-023-02285-4
41. Pierdomenico M, Negroni A, Stronati L, et al. Necroptosis is active in children with inflammatory bowel disease and contributes to heighten intestinal inflammation. *Am J Gastroenterol*. 2014;109(2):279–287. doi:10.1038/ajg.2013.403
42. Zhang C, He A, Liu S, et al. Inhibition of HtrA2 alleviated dextran sulfate sodium (DSS)-induced colitis by preventing necroptosis of intestinal epithelial cells. *Cell Death Dis*. 2019;10(5):344. doi:10.1038/s41419-019-1580-7
43. Dömling A, Holak TA. Balinatunfib: a clinical oral small molecule TNFα inhibitor. *ChemMedChem*. 2025;20(14):e202500258. doi:10.1002/cmdc.202500258
44. Yang W, Tao K, Wang Y, et al. Necrosulfonamide ameliorates intestinal inflammation via inhibiting GSDMD-mediated pyroptosis and MLKL-mediated necroptosis. *Biochem Pharmacol*. 2022;206:115338. doi:10.1016/j.bcp.2022.115338